LBL--24217

DE88 003859

The Beta Decay Asymmetry Parameter of ^{35}Ar

James David Garnett

(Ph.D. Thesis, completed 12 November 1987)

Lawrence Berkeley Laboratory
University of California
Berkeley, California 94720

This work was supported by the Director, Office of Energy Research, Office of Basic Energy Sciences, Nuclear Science Division of the U.S. Department of Energy under Contract No. DE-AC03-76SF00098.

Table of Contents

List of Figures & Tables

Chapter Two

Chapter Three

The Beta Decay Asymmetry Parameter of ^{35}Ar

James David Garnett

(Ph.D. Thesis)

Lawrence Berkeley Laboratory
University of California
Berkeley, California 94720

ABSTRACT

The beta decay asymmetry parameter for $^{35}Ar \Rightarrow {}^{35}Cl + e^+ + \nu_e$ has been remeasured in order to resolve a long standing puzzle. Previous asymmetry measurements, when combined with the comparative half-life, yield a value for the vector coupling constant, G_v, that is in serious disagreement with the accepted value. We produced polarized ^{35}Ar by a (p,n) reaction on ^{35}Cl using the polarized proton beam provided by Lawrence Berkeley Laboratory's 88-Inch Cyclotron. The polarization of the ^{35}Ar was determined by measuring the asymmetry of the positrons produced in ^{35}Ar decay to the first excited state in ^{35}Cl (branching ratio=1.3%) in coincidence with a 1219.4 keV gamma ray. Our result, $A_0 = 0.49 \pm 0.10$, combined with the comparative half-life yields a value for G_v in agreement with the accepted value.

Chapter One

Introduction

This thesis describes a measurement of the beta decay asymmetry parameter of polarized ^{35}Ar. Part A of this chapter provides the motivation for undertaking the experiment and part B describes the experimental method in broad outline.

A. Nuclear Beta Decay and Argon-35

The interaction for nuclear beta decay is given by :

$$H_{int} = \frac{1}{\sqrt{2}} G_{\mu} \bar{e}\gamma^{\lambda}(1-\gamma_5)\nu_e \, \bar{u}\gamma_{\lambda}(C_v - C_a\gamma_5)d(\cos\theta_1) + h.c.$$

where C_V and C_a are strong corrections to the hadronic current and $\cos\theta_1$ is the cosine of the Cabibbo weak mixing angle introduced phenomenologically to explain the reduced amplitude for semi-leptonic decays compared to the purely leptonic muon decay :

$$|d\rangle_{weak} = |d\rangle\cos\theta_1 + |s\rangle\sin\theta_1$$

$G_{\mu} = G_F$ is the muon decay coupling constant which is used for comparison with the semi-leptonic decays in order to extract a value for the Cabibbo angle.

The "conserved vector current" hypothesis implies $C_V = 1$, i.e. the vector coupling constant for hadronic currents is unrenormalized after strong corrections. The CVC hypothesis is tested by experimentally measuring the vector coupling constant for a variety of semi-leptonic decays. It is common to define,

$$G_V \equiv G_\mu C_V \cos\theta_1$$

$$G_a \equiv G_\mu C_a \cos\theta_1$$

for nuclear beta decays.

Confirmation of the CVC hypothesis is the statement, in this context, that G_V is independent of the nucleus considered. The constancy of G_V can also be interpreted as constancy of θ_1, known as "Cabibbo universality". To the extent that radiative corrections can be precisely calculated, Cabibbo univerality has been confirmed in the K^+_{e3} decays, hyperon β-decays, and the superallowed, $0^+ \Rightarrow 0^+$, pure Fermi transitions in nuclear β-decay. The value $\theta_1 = 0.233 \pm 0.011$ (radians) determined from the pure Fermi transitions agrees well with the value $\theta_1 = 0.229 \pm 0.016$ determined from the high energy semi-leptonic hyperon decays[1,2].

A value for the Cabibbo angle can also be determined from the mixed,

$J(\neq 0) \Rightarrow J$, $T = 1/2$ mirror transitions; however, an auxiliary measurement must be performed to determine the axial vector matrix element in each case. This can be done from an angular correlation experiment between, for example, the emitted electron or positron's momentum and the initial nuclear spin, $A\langle J_i \rangle \cdot p_e$ (Ref.3). The constant A is known as the beta decay asymmetry parameter and is related to the axial vector matrix element $\langle\sigma\rangle$ by[3],

$$A = \frac{\pm\kappa\rho^2 - 2\rho\left(\frac{J_i}{J_i + 1}\right)^{1/2}}{1 + \rho^2}$$

$$\kappa = \begin{cases} 1 & J_f = J_i - 1 \\ (J_i + 1)^{-1} & J_f = J_i \\ J_i(J_i + 1)^{-1} & J_f = J_i + 1 \end{cases} \qquad \pm \text{ for } e^{\pm}$$

where $\rho = G_a\langle\sigma\rangle/G_v\langle 1\rangle$, $\langle 1\rangle$ is the Fermi matrix element which can be precisely calculated, and we have assumed T invariance. When ρ is combined with the comparative half-life ft, G_v can be calculated :

$$(1 + \Delta_R)G_v^2 = \frac{k}{ft(1 + \delta_r)(1 - \delta_c)(1 + \rho^2)}$$

where $k = 2\pi^3(h/2\pi)^7c^6/(m_ec^2)^5$, δ_c is a correction for the imperfect isospin symmetry, δ_r is a nucleus-dependent radiative correction, and Δ_R is a nucleus-independent radiative correction[4,5,6].

The asymmetry parameter has been measured for only three nuclei: ^{35}Ar, ^{19}Ne, and ^{1}n. The derived values for θ_1 from ^{19}Ne and neutron (both spin 1/2) are 0.27±0.05 and 0.232±0.014 respectively, in agreement with the accepted value[5]. However $A_0(^{35}Ar)$ has remained anomalous for many years despite repeated measurements of all relevant parameters[7,8]. The data yield $\theta_1 < 0.10$ (95% confidence)[8].

A mechanism to decouple the down and strange quarks with a strong magnetic field was proposed by Salam and Strathdee[9]. Towner and Hardy[5] pointed out that this may be the explanation of the ^{35}Ar anomaly; perhaps the magnetic field associated with the spin 3/2 ^{35}Ar nucleus is sufficient to decouple the down and strange quarks[10]. However, a recent measurement of the comparative half-life for the transition $^{24}Al(4+)\Rightarrow{}^{24}Mg(4+)$ resulted in a value of θ_1 consistent with the pure Fermi transitions[11]. (For this transition, $\rho \cong 0$ so an auxiliary measurement to determine ρ is unnecessary.) In an attempt to resolve this problem, we have performed a remeasurement of the beta decay asymmetry

parameter of ^{35}Ar by a different experimental method.

B. A Brief Outline of the Experiment

The transition rate for allowed nuclear beta decay in the impulse approximation[12], integrated over neutrino momentum is,

$$dW = \frac{G_v^2(1+\rho^2)\,|\langle 1\rangle|^2}{\pi(2\pi)^3} F(Z,E_e)E_e p_e(\Delta - E_e)^2 dE_e\left(1 + A\frac{\langle J_i\rangle\cdot p_e}{J_i E_e}\right)$$

where $F(Z,E_e)$ is the Coulomb correction for the outgoing beta particle and Δ is the difference in the initial and final nuclear energy levels, equal to the endpoint energy of the emitted beta particle. An experiment to measure the angular correlation between J_i of the nucleus and p_e of the beta particle determines the asymmetry parameter A.

For $^{35}Ar(3/2+) \Rightarrow {}^{35}Cl(3/2+) + e^+ + \nu_e$, the asymmetry parameter A_o is given by,

$$A_o = \frac{\frac{2}{5}\rho^2 - \sqrt{\frac{12}{5}}\rho}{1+\rho^2}$$

The experiment is performed by obtaining a gas of polarized ^{35}Ar, from a (p,n) reaction on ^{35}Cl using polarized protons, and measuring the fore/aft asymmetry of the emitted positrons. The angular dependence of the positrons is given by

$W(\alpha) = 1 + A_0 P(v/c)\cos\alpha$, where $P \geq 0$ is the polarization of the ^{35}Ar nuclei, α is the angle between the positron momentum and the initial nucear spin, and v is the velocity of the emitted positron.

The ^{35}Ar gas is inside a target cell immersed in a uniform magnetic field that defines the spin axis (vertical). Above and below the target are located plastic scintillation detectors that record the number of positrons emitted from the polarized gas. The quantity measured is

$$\Delta = \left[\frac{N_+ - N_-}{N_+ + N_-}\right]_{top} - \left[\frac{N_+ - N_-}{N_+ + N_-}\right]_{bottom} = GAP$$

where N_+ or N_- is the number of counts in a given β detector for argon polarization plus or minus, respectively, and G is a sum of top and bottom detector geometry factors that includes the v/c energy dependence in the angular distribution. For the positron decay to the ground state of ^{35}Cl,

$$\Delta_o = G_o A_o P$$

while for the positron decay to the first excited state of ^{35}Cl, for which the asymmetry parameter is $A_1 = 1$ (a pure Gamow-Teller transition $3/2^+ \Rightarrow 1/2^+$),

$$\Delta_1 = G_1 P$$

hence

$$\frac{\Delta_0}{\Delta_1} = A_0 \frac{G_0}{G_1} \cong A_0$$

The ratio is independent of the argon polarization and allows a determination of the asymmetry parameter A_0 up to the ratio of geometry factors which is very nearly unity. The positrons associated with the first excited state of ^{35}Cl are separated from the much larger groundstate contribution by a coincidence requirement with a 1219 keV gamma ray (see Figure 1, chapter 2).

The crucial feature of the experiment is the measurement of the first excited-state decay of ^{35}Ar that calibrates the polarization of the Argon gas. The ratio Δ_0/Δ_1 also removes many possible systematics, the ratio depending only on the *change* in the value of the systematic due to the difference in the endpoint energies of β_0 (the groundstate decay) and β_1 (the first excited-state decay).

references

[1]E. A. Paschos and V. Turke, Phys. Lett. **116B**(1982)360

[2]M. Roos, Nucl. Phys. **B77**(1974)420

[3]J. D. Jackson, S. B. Trieman, and H. W. Wyld, Phys. Rev. **106**(1957)517

[4]I. S. Towner and J. C. Hardy, Nucl. Phys. **A254**(1975)221

[5]J. C. Hardy and I. S. Towner, Phys. Lett. **58B**(1975)261

[6]A. Sirlin, Rev. Mod. Phys. **50**(1978)573

[7]G. L. Wick, D. C. Robinson, and J. M. Freeman, Nucl. Phys. **A138**(1969)209 and Phys. Lett. **30B**(1969)240

[8]E. Hagberg, J. C. Hardy B. Jonson, S. Mattsson, and P. Tidemand-Petersson, and the ISOLDE Collaboration, Nucl. Phys. **A313**(1979)276

[9]A. Salam and J. Strathdee, Nature **252**(1974)569 and Nucl. Phys. **B90**(1975)203

[10]P. Suranyi and R. A. Hedinger, Phys. Lett. **56B**(1975)151

[11]E. G. Adelberger, P. B. Fernandez, C. A. Gossett, J. L. Osborne, and V. J. Zeps, Phys. Rev. Lett. **55**(1985)2129

[12]See, for example, E. D. Commins and P. H. Bucksbaum, Chapter 5, Weak Interactions of Leptons and Quarks, Cambridge University Press, 1983, and references therein.

Chapter Two

The Experiment

This chapter describes the experimental set-up in detail. Part A describes some design criteria, part B describes the system in detail, and part C summarizes the cyclotron runs and detector performances.

A. Design Criteria

Contaminants are a serious problem in any accelerator experiment where beta spectra are involved. The low resolution of plastic scintillators and the broad energy spectrum from beta radiation can easily mask the presence of other particles. Table 1 is an extensive tabulation of possible contaminants with $Q \leq 12MeV$[1,2]; the target elements are chosen from consideration of the materials the proton beam may intercept. Many potential contaminants can be removed by maintaining the beam's energy below their thresholds. Low energy background can be removed by appropriate energy cuts in the data.

When the proton beam is passing through the target cell, intense neutron and gamma ray fluxes exist. Photomultiplier tubes will have higher dark currents and gain drifts after plastic detector exposure to the intense gamma ray and neutron fluxes. Solid-state detectors are damaged by neutron induced dislocations in the crystal, resulting in poorer resolution. To protect phototubes, the high voltage can be gated or a shutter system can be installed. Gating the

Table 1:contaminants

Target	Reaction	Product	Q(MeV)	$t_{1/2}$	Radiations
$_9F^{19}$	(p,n)	$_{10}Ne^{19}$	4.02	17.4s	β^+ (2.2 MeV)
	(p,d)	$_9F^{18}$	8.21	110m	β^+ (0.64 MeV)
	(p,t)	$_9F^{17}$	11.1	66s	β^+ (1.7 MeV)
	(p,α)	$_8O^{16}$	-8.12	stable	
	(p,γ)	$_{10}Ne^{20}$	-13.2	stable	
$_{17}Cl^{37}$	(p,n)	$_{18}Ar^{37}$	1.60	35d	Cl x-rays (EC)
	(p,2n)	$_{18}Ar^{36}$	10.4	stable	
	(p,d)	$_{17}Cl^{36}$	8.09	$3x10^5$y	
	(p,t)	$_{17}Cl^{35}$	10.4	stable	
	(p,He^3)	$_{16}S^{35}$	10.6	88d	β^- (0.167 MeV)
	(p,α)	$_{16}S^{34}$	-3.03	stable	
	(p,γ)	$_{18}Ar^{38}$	-10.2	stable	
$_{17}Cl^{35}$	(p,n)	$_{18}Ar^{35}$	6.75	1.76s	our reaction
	(p,d)	$_{17}Cl^{34}$	10.4	1.56s	β^+ (4.46 MeV)
	(p,He^3)	$_{16}S^{33}$	10.1	stable	
	(p,α)	$_{16}S^{32}$	-1.86	stable	
	(p,γ)	$_{18}Ar^{36}$	-8.51	stable	
$_6C^{12}$	(p,γ)	$_7N^{13}$	-1.94	10m	β^+ (1.2 MeV)
$_6C^{13}$	(p,n)	$_7N^{13}$	3.00	10m	β^+ (1.2 MeV)
$_6C^{13}$	(p,d)	$_6C^{12}$	2.72	stable	
	(p,α)	$_5B^{10}$	4.06	stable	
	(p,γ)	$_7N^{14}$	-7.55	stable	
$_8O^{16}$	(p,He^3)	$_7N^{14}$	11.24	stable	
	(p,α)	$_7N^{13}$	5.22	10m	β^+ (1.2 MeV)
	(p,γ)	$_9F^{17}$	-0.60	67s	β^+ (1.74 MeV)
$_8O^{17}$	(p,n)	$_9F^{17}$	3.54	67s	β^+ (1.74 MeV)
	(p,d)	$_8O^{16}$	1.92	stable	
	(p,t)	$_8O^{15}$	11.3	124s	β^+ (1.7 MeV)
	(p,He^3)	$_7N^{15}$	8.55	stable	
	(p,α)	$_7N^{14}$	-1.19	stable	

Target	Reaction	Product	Q(MeV)	$t_{1/2}$	Radiations
$_8O^{17}$	(p,γ)	$_9F^{18}$	-5.61	110m	β^+ (0.635 MeV)
$_8O^{18}$	(p,n)	$_9F^{18}$	2.44	110m	β^+ (0.635 MeV)
	(p,2n)	$_9F^{17}$	11.59	67s	β^+ (1.74 MeV)
	(p,d)	$_8O^{17}$	5.82	stable	
	(p,t)	$_8O^{16}$	3.71	stable	
	(p,α)	$_7N^{15}$	-3.98	stable	
	(p,γ)	$_9F^{19}$	-7.99	stable	
$_7N^{14}$	(p,n)	$_8O^{14}$	5.927	70.6s	β^+ (1.8 MeV 99%)
					γ (2.31 MeV 99%)
	(p,d)	$_7N^{13}$	8.328	10m	β^+ (1.2MeV)
	(p,He^3)	$_6C^{12}$	4.78	stable	
	(p,α)	$_6C^{11}$	2.92	20.4m	β^+ (0.961 MeV)
	(p,γ)	$_8O^{15}$	-7.29	122s	β^+ (1.72 MeV)
$_7N^{15}$	(p,n)	$_8O^{15}$	3.54	122s	β^+ (1.72 MeV)
	(p,d)	$_7N^{14}$	8.61	stable	
	(p,He^3)	$_6C^{13}$	10.67	stable	
	(p,α)	$_6C^{12}$	-4.96	stable	
	(p,γ)	$_8O^{16}$	-12.1	stable	

high voltage has the disadvantage of requiring time for the tube gain to stabilize and will not protect the photocathode from possible damage. Shutters will inevitably result in reduced light input to the photocathode. Neutron damage to solid-state detectors can be ameliorated by shielding with borated water and polystyrene but beyond this, damage is unavoidable.

Good detector efficiency for the positrons demands plastic scintillators, as large and as close to the target cell as possible. The choice for gamma ray

detectors is less straightforward. The two main candidates are NaI(Tl) and solid-state high purity Germanium. The former has excellent efficiency but very poor resolution, approximately 8% at 1 MeV. The latter has poorer efficiency but excellent resolution, approximately 2 keV at 1 MeV. If efficiency were the only consideration, then NaI would be the logical choice; but resolution is important because of positron annihilation-in-flight background which reduces the signal to noise and increases collection time.

The target cell material must be able to withstand an atmosphere of pressure and possible corrosive effects from chlorine, but be thin enough to allow transmission of the positrons. It must not produce unacceptable background when the proton beam strikes the entrance and exit foils. Finally, it must be a low Z material to minimize positron backscatter, which tends to wash out any asymmetry. These considerations lead to the use of strong acrylic plastics such as lucite or mylar.

The low branching ratio of the first excited state, used to calibrate the polarization, leads to some problems. Because of the low activity it is preferable to use the most efficient detectors and produce a large amount of ^{35}Ar. The amount of Argon produced depends on the proton beam energy (the cross section for production is energy dependent) and current as well as the pressure of the target gas; unfortunately, the beam parameters are constrained by other considerations: the energy must be below the ^{34}Cl production threshold of 10.4

MeV (see Table 1) and the beam current must not be so high as to rupture the very thin entrance and exit foils of the target cell by overheating. If solid-state detectors are used there is the additional consideration of how much neutron damage one is willing to tolerate. Higher beam current means greater damage from (p,n) reactions in the mylar entrance and exit foils for the same amount of run time. This leaves the target gas as the best parameter to increase ^{35}Ar production.

Ideally, one wants an alkyl chloride with a large chlorine to molecule ratio and a high vapor pressure. One of the best candidates is carbon tetrachloride, CCl_4. It has one of the largest fractions of chlorine per molecule and also has a reasonable vapor pressure, 90 torr at about 20°C. The only serious contender of the alkyl chlorides is methylchloride, CH_3Cl. Methylchloride is a gas at room temperature, which more than compensates for the single chlorine atom per molecule (although it is found experimentally that one must operate at well below an atmosphere to prevent unacceptable scattering of the proton beam), but is unuseable because it is highly inflammable and very toxic.

The only other serious candidates are the fluorochlorocarbons, more commonly known as freons. The best candidate of the freons is freon-11, fluoro,trichloromethane, $CFCl_3$. It is noncombustible and has a vapor pressure of approximately 650 torr at 20°C. Its main disadvantage is the contamination

produced from reactions involving Fluorine (see Table 1).

Low vapor pressure can be overcome to some extent by heating the storage can, but too much heat will only result in the gas condensing in the target cell (and heating the entire apparatus is difficult). Solid or liquid targets are excluded due to positron diffusion and backscattering problems.

B. Description of Experiment

a. Overall description

A 5 nanoamp beam of 10 MeV polarized protons, average polarization ≅ 50%, was obtained from the LBL 88-Inch Cyclotron. The beam energy was chosen to lie above the 6.7 MeV threshold for ^{35}Ar production by a (p,n) reaction on ^{35}Cl, but below the 10.4 MeV threshold for ^{34}Cl production by a (p,d) reaction on ^{35}Cl. ^{34}Cl has a similar positron endpoint energy and half-life to ^{35}Ar and was the only potentially troublesome contaminant close to the argon threshold.

The protons entered a hollow lexan target cell (9.5cm×11.4cm×7.0cm) containing a He+CCl_4 gas mixture at 470 and 95 torr, respectively, through a 0.013cm mylar entrance foil (3.2cm diameter). The reaction $^{35}Cl(p,n)^{35}Ar$ proceeded with a polarization transfer of approximately 12%, resulting in an ^{35}Ar polarization of (6±1)%[3]. The proton beam left the target cell through a mylar exit foil and was stopped in a shielded carbon block far downstream from the cell.

The proton beam's polarization was measured before and after the run

using a carbon-foil polarimeter. The stability of the polarization was monitored during the run by the stability of the asymmetry for the decay to the ground state of ^{35}Cl. The polarization remained stable to within 12% for almost 80% of the 48 hour run and to within 20% for the entire run. This drift in polarization is not important in our experiment because we measure the polarization by our asymmetry measurement of ^{35}Ar decay to the first excited state of ^{35}Cl. When the proton beam was unpolarized, the asymmetry of ^{35}Ar vanished.

The target was inside a uniform magnetic field of 30G, produced from a pair of Helmholtz coils, that maintained the ^{35}Ar polarization during the counting period. The polarization was found to rise quickly from zero and then level off as the magnetic field was increased from zero to 30G. The Helium acted as a buffer to slow diffusion of the Argon gas to the target cell walls, where depolarization may have occured. No systematic effect was observed when the magnetic field was reversed midway through the run.

The positrons from the target passed through 0.025cm mylar foils (9.5cm×11.4cm) on the top and bottom of the cell. They were detected in a ΔE-E telescope system, consisting of plastic scintillator detectors, located above and below the target cell (see Fig. 1). Lightpipes transported the scintillation light to photomultiplier tubes located well outside the magnetic field region. A ΔE scintillation detector (10.2cm×10.2cm×0.16cm) was situated between the target

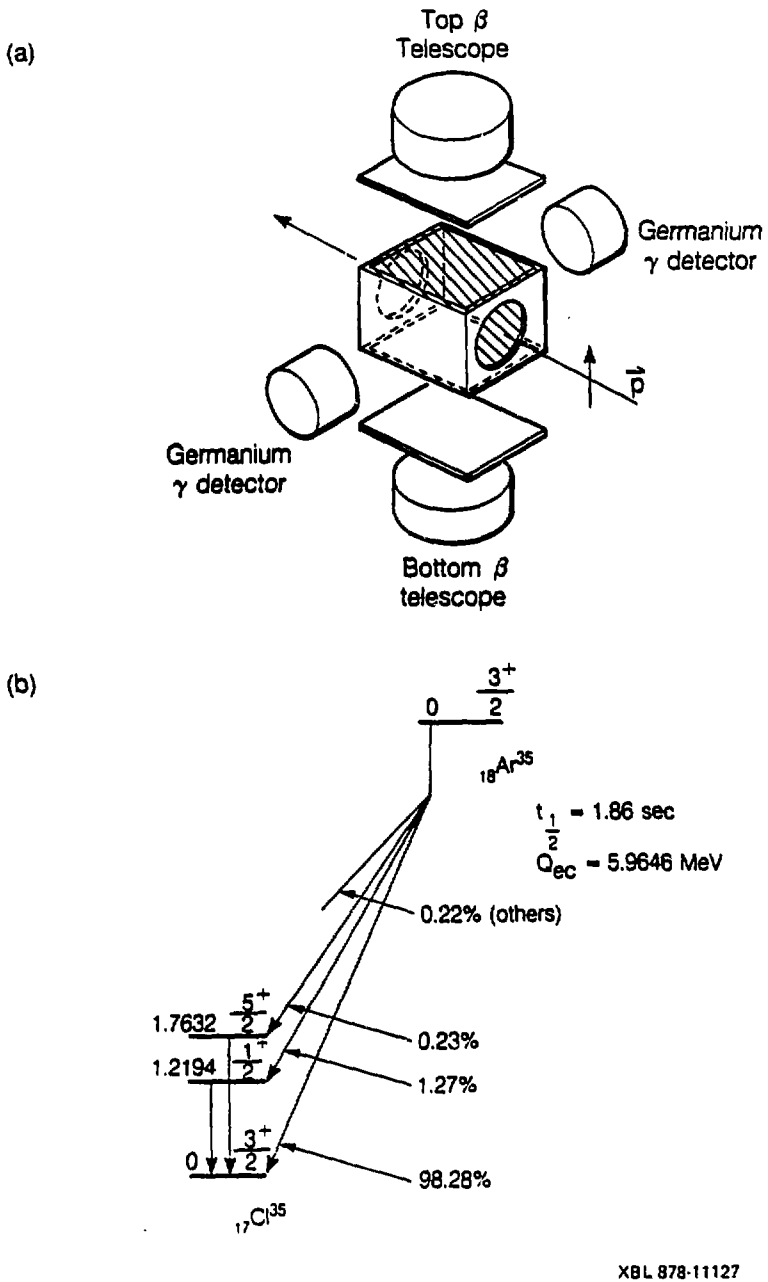

Fig. 1(a) Schematic of the experimental set-up

1(b) The decay scheme of Argon-35

cell and each positron E-detector (10.2cm diameter × 3.8cm thick). A valid detector signal only occurred when there was a coincidence between the E detector and its associated ΔE detector. This arrangement suppressed gamma ray signals and noise in the main detectors. An anti-coincidence between opposite E-detectors eliminated positrons which backscattered from one detector into the other.

The positrons associated with the decay to the first excited state of ^{35}Cl (branching ratio ≅ 1.3%) were distinguished from the ground-state signal (branching ratio ≅ 98.3%) by a coincidence requirement with a 1219.4 keV gamma ray. To treat the ground-state signal analogously to the excited-state signal, coincidence with a 511 keV annihilation gamma ray was required. A prompt coincidence was obtained when a positron came to rest in an E-detector and annihilated.

The gamma rays were detected by two high purity Germanium detectors. Each detector has an active volume of 109cm^3 and an efficiency of approximately 25% compared to a 7.6cm×7.6cm NaI(Tl) detector (as outlined in the IEEE Test Procedures for Ge Detectors for Ionizing Radiation, ANSI/IEEE 325-1986). The Germanium detectors were chosen, in the final runs, instead of higher efficiency NaI detectors, to suppress detection of gamma rays from annihilation-in-flight positrons in the plastic detectors. These positrons produce a prompt coincidence

with their annihilation-in-flight gamma rays. The contribution from these events to the coincidence of positrons with a gamma ray in an energy acceptance window of 8 keV centered about 1219 keV was ~10%. The contribution to the much poorer resolution NaI detectors would be unacceptably high.

A microcomputer controlled the system, which was sequenced through a series of steps every 9.55 seconds. The proton beam was sent into the target for 3.2sec and then blocked with a beam stop. During a delay of 150msec, mechanical camera shutters, located between the lightpipes and photomultiplier tubes of the positron E-detectors, were opened. The shutters protected the phototubes from the intense light generated when the proton beam was on. During this same delay the high voltage was gated on to the ΔE photomultiplier tubes. A 3.2sec counting period ensued, after which the target was pumped out for 2.0sec and then refilled with fresh gas for 1.0sec. The polarization of the beam was then reversed and the entire sequence was repeated. The beam on and data collection times were chosen to maximize counting efficiency; the delay was chosen to provide enough time to charge the voltage divider of the ΔE tubes and allow the camera shutters to fully open; the pump out and fill times were chosen as the fastest times possible to allow thorough evacuation of the used gas and proper filling with the fresh gas.

b. Electronics

The electronics design is shown in Fig. 2. The basic design can be divided

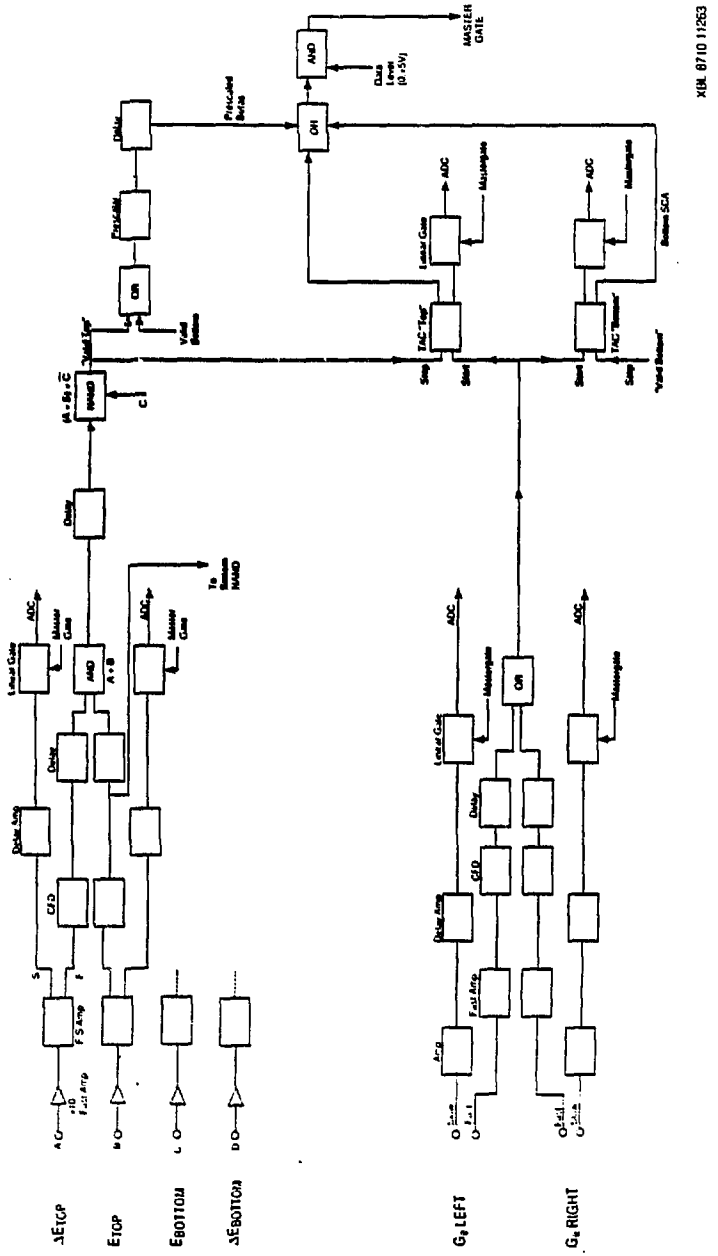

Fig. 2 Schematic of the electronics

into two categories: generation of a slow energy signal from each detector and generation of a fast timing signal for coincidence between the plastics and Germanium detectors.

Each of the four plastic detector signals is sent into a ×10 fast preamp and then into a combination fast/slow amplifier. The slow channel signal is sent to a linear gate which requires a master gate signal before sending a shaped pulse to the analog to digital (AtoD) converter. The latter interfaces with the DEC-MODCOMP computer of the 88-Inch Cyclotron. The fast channel signal goes to a constant fraction discriminator (CFD) where a precise fast negative timing signal is generated. The timing signals from the top or bottom E+ΔE detectors are logically AND'ed (the E-ΔE coincidence requirement) and then this new (fast negative) signal is sent to a logical VETO unit which will veto the signal if a fast timing signal from the CFD of the opposite E-detector is present within an approximately 40ns time window (the anti-coincidence between top and bottom). If there is no veto, then a valid fast negative signal from the top or bottom plastic detector system is generated and sent to the time to amplitude converter (TAC).

Each Germanium detector has its own preamplifier system which generates two signals, one for the slow channel and one for the fast channel. The slow channel signals are amplified and sent to a linear gate, the same as with the plastic slow signals. The fast signals are sent into CFDs and then logically OR'ed

before being sent to the START inputs of the TACs for the top and bottom systems.

The TACs are set at a 200ns time range and require a STOP signal from the appropriate beta detector system to produce an output signal. The TACs generate two signals if a STOP signal is received within 200ns from the time of the START signal: a 0-10V signal that is a linear function of the time separation between the start and stop signals and a positive 5V signal. The time signal is sent to a linear gate which sends the signal to the AtoD when the master gate is received. The +5V signal is involved in the generation of a master gate.

The master gate is generated during the data collection whenever a timing event is recorded by either of the TACs or whenever a (prescaled) singles event is received from the top or bottom plastic detector system. This is accomplished by a logical OR between the prescaled valid top or bottom signals and the TAC +5V signals. This output is logically AND'ed with a +5V data collection level from the microcomputer in control of the system to insure that a master gate only occurs during data collection. This signal becomes the master gate for the slow energy signals as well as for the two TAC timing signals and the proton polarization signal.

The prescaler is used to keep the information transfer rate to the computer at an acceptable level. The peak activity the system can handle and still write to magnetic tape and interact with the experimenters in real time is ~10^5/N events

per second, where N is the number of channels into the AtoD. For our experiment, N = 9 so the peak activity is ~10^4events/sec. The beta singles activity was typically ~10^4sec^{-1}. The prescale factor was chosen to be 129.

In addition to this system, a dead time monitor system is also present (not shown in Fig.2). It involves sending a valid top or bottom plastic fast signal to a scaler and to the gate of a discriminator. The input to the discriminator is the appropriate top or bottom slow energy signal and if this signal is present when the gate is present, a standard +5V signal is generated which is recorded by another scaler. The comparison of these two scalers, a pair for both the top and bottom systems, provides dead time information on the top and bottom detectors. This system only monitors the deadtime associated with the slow channel, but this is the dominant source of dead time. It also does not monitor the dead time associated with the AtoD, but this is common to all the detectors and is not important for the way the asymmetry is calculated.

c. Detectors

Positrons are detected with Bicron® BC-404 plastic scintillation detectors. The plastic consists of a polyvinyltoluene base with a few percent addition of a primary fluorescent compound, p-terphenyl, and a wave shifter compound, 4,4'-diphenylstilbene[4]. The primary fluorescent shortens the decay time of the material and increases the light conversion efficiency. The wave shifter makes the plastic more transparent to its own light and better matches the spectral

response of bialkali tubes. It is the aromaticity of the constituents that distinguishes organic scintillators from ordinary acrylic plastics, such as mylar or lucite. BC-404 has an absolute light conversion efficiency of approximately 2%[5], with a wavelength of maximum emission at 408nm. The 1.8ns decay constant makes this plastic ideal for fast counting.

The positron detection system is a ΔE-E telescope configuration. The 10.16cm ×10.16cm ×0.16cm plastic "wafer" ΔE-detector, located between the target cell and main E-detector, is used to veto gamma rays and noise in the main detector by a coincidence requirement between the ΔE and E detectors. The overall detection efficiency for 511 keV gamma rays in the thin plastic is only ~1-2%[6] compared to essentially 100% response to beta radiation. The main detectors are 10.16cm diameter cylinders, 3.81cm thick. The thickness is chosen to insure complete energy collection for all positrons emitted from ^{35}Ar; a 3.8cm thickness is the range for 7.5 MeV betas.

The scintillation light from the plastics is transported tc RCA 8575 photomultiplier tubes by lucite lightpipes. The ΔE-detector is epoxied to a lightpipe ledge and buttressed against an approximately 10.2cm ×0.16cm wall which gradually transforms to a 5.08cm diameter cylindrical rod that sits against the photocathode. The E-detector is epoxied to a 10.16cm diameter lightpipe face that tapers to a 5.08cm diameter. The 5.08cm end fits into an aluminum

flange that also holds the mechanical camera shutter. On the other side of the shutter system, another aluminum flange holds a second lightpipe, a 5.08cm diameter, 0.91m long cylindrical rod. Both lightpipes sit in central wells in the flanges, facing the overlapping leaves of the 5.08cm diameter shutter, and are held in place by three transverse screws. The three foot long cylindrical rod is bent so that the two end faces define planes at 90° to one another. The second face is butted against a photocathode. The bend was achieved by uniformly and slowly heating a three foot rod of lucite for about 20 minutes until it became pliable. The rod was quickly bent into the desired curve and clamped until it cooled.

The detectors and lightpipes are wrapped with Al foil to maximize light collection and then with electrician's tape to seal against light leaks. The lightpipes transport the scintillation light to the phototubes which lie well outside the magnetic field region of the Helmholtz coils. The camera shutter assembly, which is controlled by a solenoid, is also removed from the proximity of the photocathodes and carefully assembled to prevent light leaks. The shutter system for the main detectors reduces the light output by approximately 30% compared to the system without the assembly. To protect the ΔE-detectors during beam on, the high voltage is gated to the voltage divider string. Gain drift is not a problem for the ΔE-detectors which only serve as noise and gamma ray vetos.

The gamma rays are detected with high purity, coaxial Germanium detectors with an active volume of 109cm^3. The detectors are part of the EG&G Ortec® GMX series, which are N-type crystals providing extra protection to neutron radiation damage. The N-type crystal can withstand almost 25 times the total neutron bombardment of a conventional p-type crystal before damage is evident. At approximately 10^{10} neutrons/cm^2 damage begins to be noticeable, and the resolution is worse by a factor of two at ~10^{11} neutrons/cm^2(Ref. 7). The photopeak efficiency for a 1.33 MeV gamma ray is 27% relative to 7.6cm×7.6cm NaI(Tl), using a ^{60}Co source located 25 cm, along the axis of symmetry, from the face of the detector.

d. Target cell and polarimeter

The final design of the target cell was arrived at by trial and error, with three previous target cell constructions before this target cell. It is a combination of lexan and mylar construction. The basic frame is a hollow lexan box with four walls, but open on the top and bottom. The lexan shell has outer dimensions 9.53cm wide×11.4cm long×6.99cm high with wall thickness 0.79cm. The front and back walls have 3.8cm diameter holes cut through them to allow passage of the proton beam. One back corner is faced and a 0.64cm gas line entrance is drilled and tapped.

Thin mylar foils are used to seal the target from the air. 9.5cm×11.4cm mylar

foils, 0.025cm thick, are epoxied to the top and bottom faces of the cell. To insure strength, plastic braces are epoxied to the foils and screwed into the lexan perimeter surface. The thin mylar foils allow nearly 100% transmission of positrons with only about 50 keV energy loss. 5.1cm diameter foils, 0.013cm thick, are used to seal the entrance and exit portals. The foils are pressed against viton O-rings, concentric to the portals, with plastic braces that are screwed into the lexan walls. The foils can tolerate a 5-10na beam of 10 MeV protons for extended periods of time without rupturing. The protons lose approximately 600 keV passing through the first foil and 700 keV passing through the second. The target cell can hold a vacuum as well as overpressures up to one atmosphere.

Plastic flanges that mate to the beampipes are epoxied to the portal walls of the target cell. The front flange mates to the beamline and the back flange mates to an Aluminum pipe about one meter long, 10.16cm inner diameter, that attaches to the carbon-foil polarimeter. The polarimeter is made out of a cylindrical, hollow brass body with two hollow arms jutting off the main body at 70° to the central axis (with the back of the polarimeter defined as 0°). Inside the main chamber of the polarimeter is a thin carbon foil, perpendicular to the proton beam. Behind the foil is a carbon block beam stop. Protons are scattered from the carbon foil and those scattered at 70° travel down the arms to solid-state

Silicon detectors where they are detected. The asymmetry in counts between the two detectors is a measure of the proton polarization.

(At 70° with a ~0.0045cm carbon foil, scattering 8.7 MeV protons, the analyzing power is fairly high, ~0.85. This was what guided our design of the polarimeter. The polarimeter helped us to maximize the polarization of the beam during the tuning of the polarized ion source. It was a crude device that couldn't separate the elastically scattered protons from the inelastic ones. For the test run prior to our final run we first sent the beam into another cave containing a very sophisticated He-polarimeter [θ_{lab} = 108.8°, E_{proton} = 5 MeV, analyzing power = .95-1.00]. This served to calibrate our own polarimeter. During the final run, the stability of the polarization was monitored by the ground state asymmetry for positron emission. At the end of the run a final polarization reading was taken with our polarimeter. The proton polarization remained stable to within 12% for most of the run.)

e. Gas handling and computer system

Gas is delivered to and pumped from the target cell by the gas handling system shown in Figure 3. Helium, at ~3/4 atm pressure, is bubbled through CCl_4 stored in a six liter stainless steel cannister, approximately 13″ high with a 6″ diameter. Bubbling the helium through the liquid carbon tetrachloride helps to transport the carbon tetrachloride to the target when the fill valve (#2 in Fig.3) is

opened. The target pressure is monitored by a dry filled pressure gauge,

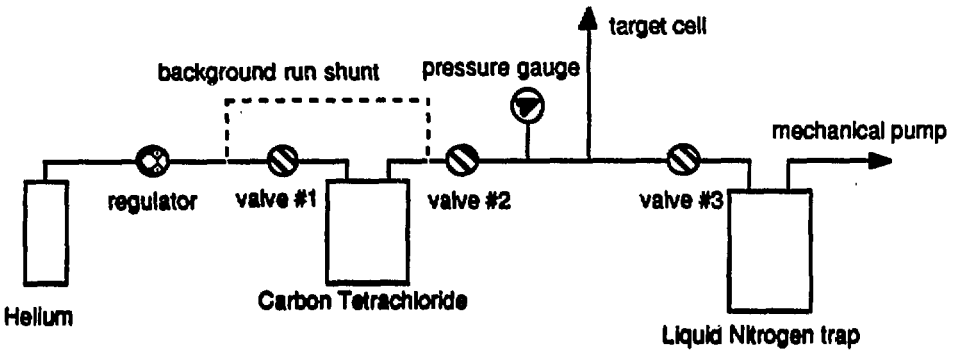

Figure 3. Gas handling system.

30"-0-15psi, that is viewed remotely in the counting area. The target is pumped by a mechanical pump that follows a liquid nitrogen trap used to freeze out the CCl_4 and related decomposition products. The trap consists of a steel cannister, similar to the storage can, cooled by liquid nitrogen in a dewar that is filled automatically by a thermocouple monitor.

The CCl_4 is delivered to the target at vapor pressure (~90 torr at 20°C). Because the target tends to be at a higher temperature than the storage cannister it was found that the liquid CCl_4 could be heated, raising the vapor pressure, without causing condensation of CCl_4 in the target. From the activity of the excited branch (due only to ^{35}Ar) we estimate that the heating caused an increase in vapor pressure of ~30%, which would show up as a 5% increase in

the total target pressure. The storage cannister was warmed up from ~65°F to ~75°F, vapor pressure rising from ~85 torr to ~110 torr. (This increase would not be noticeable on the fairly course pressure gauge used, so the estimate could not be checked directly. Our thermocouple gauge could not respond to the rapid pump and fill sequencing used during the run.)

The sequencing of the gas handling system is performed remotely by computer control. The valves of the gas system are stainless steel two-way, normally closed, solenoid valves, rated at 50psi maximum differential pressure. They are operated by 117V ac; the line voltage is optically isolated from the 5V computer control signals.

C. The Run and Experimental Performance

All the data used to calculate the final results were obtained during a run which occurred 6-9 April 1987, Monday 4:00pm-Thursday 4:00am. The experimental conditions are tabulated in Table 2. A brief chronological review of the runs prior to the April 1987 run follows:

Academic year 1985-86: Several runs were performed to assess background, detector responses, and the data acquisition system. Many of the runs were plagued by instrument problems, both ours and those of the 88-Inch Cyclotron. During this period, NaI detectors were used to detect the 1219 keV gamma ray, but the annihilation-in-flight background due to β_0 was unacceptably high to

allow confidence in the extraction of an answer. 10.16cm×10.16cm×1.91cm pilot-B detectors were used to detect the positrons, without the ΔE veto detectors. The detector thickness was probably just acceptable, with a continuous slowing down approximation range equal to that of normally incident 4 MeV positrons. The data acquisition was limited to our own microcomputer (AIM 65/40) which communicated with the collection devices by an IEEE bus. This severely restricted the amount and variety of data we could collect.

Academic year 1986-87: For these runs, we switched to the set-up described in this chapter. The E-ΔE detectors and shutter system were not installed until the final test run, but the HPGe detectors and data acquisition system were used throughout these runs:

Sept. 26,27 1986 Run #1(test): During this run, the target leaked so a large part of the data was due to ^{14}O. We used Freon-11 gas at 1 atmosphere and the proton beam was scattered excessively. We switched to CCl_4 and clearly saw the 1219 keV line, but with a large background due to annihilation-in-flight gamma rays from both ^{14}O positrons and Compton scattered 2.3 MeV gamma rays from ^{14}O.

The ^{14}O was a serious contaminant (see Table 1) with its high energy positrons and gamma ray, and obliterated the ^{35}Ar β_0 spectrum; in addition, ^{19}Ne was a potentially serious problem but was also masked by the oxygen-14. Both

contaminants have high energy betas, 1.8 MeV and 4.1 MeV (0.6%) for ^{14}O and 2.2 MeV for ^{19}Ne.

Oct. 16,17 Run #2: Using an adjustable volume storage tank for Freon-11, before delivery to the target cell, we could control the pressure in the target. We ran with ≤1/2 atm freon. From a decay spectrum taken with a timing bin configuration, we concluded that there was a very large contribution from ^{19}Ne. There was evidence from the gamma spectrum of other contamination - ^{14}O, ^{59}Fe, ^{60}Co, and an unidentified line at 1759±1 keV.

The high purity Germanium detectors were severely damaged by the neutron flux- going from a ~2 keV resolution at 1.33 MeV before the run to ~4 keV after the run, which implies a total neutron flux over time of ~10^{11} neutrons/cm^2. This damage was almost certainly due to neutrons produced in a (p,n) reaction on ^{19}F (and ^{35}Cl) in the freon. The long run time combined with the high beam current and high target gas pressure resulted in the tremendous neutron flux over time. (The final run listed in Table 2 shows a better resolution than quoted above- it turns out the resolution can be improved somewhat by placing a very hot gamma source near the detector prior to running. Apparently this has the effect of "filling" some of the damage sites with electrons, allowing for a better collection efficiency during the run and thus a better resolution.)

There was evidence of an energy dependence to the asymmetry Δ_0 (see

chapter 3). This could not be a real physical effect and indicated a detector problem.

Nov. 7,8 Run #3: This run was plagued by low average polarization ≅25%. Because of the damage to the gamma detectors we also ran at a lower beam current ~3na. The fractional uncertainty in the asymmetry scales inversely as the polarization and square root of the beam current so we lost severely in precision and did not use the data obtained in this relatively short run.

The gamma spectra were clean, with the 511 keV, 1219 keV, and 1763 keV lines as the only prominent peaks. We saw evidence for significant 511 keV detection in the plastic detectors and decided that a thin plastic veto detector was necessary for the next run.

The energy dependence of Δ_0 was tracked down to space charge effects and fatigue of the phototubes. This problem was a combination of the HV gating which causes gain drifts, exposure of the photocathodes to the intense radiation when the beam is on, and too high a voltage applied to the phototubes for the amount of activity we observe.

Mar. 27,28 Run #4(test): The asymmetry Δ_0 was stable as a function of energy. The detectors operated properly with no evidence of fatigue or space charge build-up. The ΔE-E telescope resulted in significant reduction of the low energy end of the E spectrum.

Apr. 6-9 Run#5: Successful run. See chapter 3 for details. The experimental conditions for this run are shown in Table 2 below.

Table 2:experimental conditions

beam	target cell	run
current: 4-6na	gases: He+CCl_4	total cycles: 8993
energy:9.98 MeV	pressure: 570-610 torr	total time: 47.7 hours
polarization[8]	partial pressures	duty cycle: 1/3
beginning: 0.46±0.01	CCl_4~100 torr	
ending: 0.52±0.02	He~500 torr	

raw counts

β_0 with 511 keV coincidence[9]:
TOP 578090
BOTTOM 687791

β_1 with 1219 keV coincidence[9]:
TOP 7402
BOTTOM 8356
background ~ 10%

average activity:
total activity ~ 1.5-3.5×10^4 sec^{-1}
β_0 with 511 activity ~ 23 sec^{-1}
β_1 with 1219 activity ~ 0.3 sec^{-1}

detectors

β: Bicron BC-404 (pilot-B)
HV = -1900V & -1925V
anode: ≤100mV into 50Ω

γ: EG&G Ortec HPGe (GMX series)
HV = -3000V & -4000V
~3 keV FWHM @ 1219 keV
~3.5 keV FWHM @ 511 keV

General references:

F. Adams and R. Dams, Applied Gamma-Ray Spectroscopy, 2nd edition, Oxford, New York, Pergamon Press [1970]

C. E. Crouthamel, Applied Gamma-Ray Spectroscopy, 1st edition, Oxford, New York, Pergamon Press [1960]

J. B. Birks, The Theory and Practice of Scintillation Counting, Oxford, Pergamon Press [1964]

N. Tsoulfanidis, Measurement and Detection of Radiation, New York, McGraw-Hill [1983]

G. F. Knolls, Radiation Detection and Measurement, New York, Wiley [1979]

K. Siegbahn ed., Alpha-, Beta-, and Gamma-Ray Spectroscopy, vol. 1&2, Amsterdam, North-Holland [1965]

references:

[1]C. M. Lederer, J. M. Hollander, and I. Perlman, Table of Isotopes, 6th ed., New York, Wiley [1967]

[2]N. B. Gove and A. H. Wapstra, Nuclear Data Tables A, 11 (1972) November

[3]The value is based on the measured value for A_0 and the geometry factor G_0 obtained from the Monte Carlo simulation. See text for details.

[4]J. B. Birks, The Theory and Practice of Scintillation Counting, Oxford, Pergamon Press [1964]

[5]Private communication, C. R. Hurlbut, Bicron Corporation.

[6]C. R. Hurlbut, "Plastic Scintillators: A Survey", presented at the American Nuclear Society Winter Meeting, November 1985

[7]R. H. Pehl, N. W. Madden, J. H. Elliot, T. W. Raudorf, R. C. Trammell, and L. S. Darken, Jr., IEEE Trans. Nucl. Sci., NS-26 (1979) 321

[8]The analyzing power is included. From the test run, with the He-polarimeter as calibration, I estimate the analyzing power to be 0.85-0.90.

[9]Counts above the chosen cut-offs. See chapter 3 for details.

Chapter Three

Results

This chapter describes the data, selection criteria, energy cuts, and corrections in detail.

A. Spectra

The DEC-MODCOMP computer system stored nine spectra on magnetic tape. The data collected and the divisions of the approximately 48 hours of collection time into smaller subruns are tabulated in Table 1.

Table 1a: spectra

1. Energy: ΔE top plastic
2. Energy: E top plastic
3. Energy: ΔE bottom plastic
4. Energy: E bottom plastic
5. Energy: Germanium "left"
6. Energy: Germanium "right"
7. Time: TAC spectrum γ/ΔE-E top
8. Time: TAC spectrum γ/ΔE-E bottom
9. Polarization: ± (~3V/7V)

1b: runs

Run#	Activity (10^4 sec^{-1})	Time(min.)
601	1.4	360
602	1.6	360
603	1.6	510
605	3.5	100
606	2.2	610
607	1.7	210
608	1.7	690

For subruns 607 and 608, only the activity for the sum of the two runs was determined, so the quoted value represents an average; also, for run 608 the listed time length includes ~60 minutes that were lost replacing the liquid

Nitrogen trap.

The complete energy spectra of all the detectors are collected as well as the timing between gamma rays and the top/bottom plastic detector systems. Every event is also tagged by the polarization of the beam which is recorded as one of two voltages corresponding to polarization + or -. The runs are arbitrarily divided in time. Run 604 was ended minutes after the start, so was dropped from the data. The activity is calculated from the total valid top and bottom fast plastic signals during the run, corrected for the duty cycle.

B. Derivation of A

The most general expression for the counts in a given plastic detector is:

$$N_{\pm} = C_{\pm}\Big(\int f(E)\varepsilon(E,E_c,\theta)T(E)\Big(1 \pm \frac{v}{c}P_{\pm}A\cos\theta\Big)dEd\Omega_{\beta}dVd\Omega_{\gamma} +$$

$$\int f(E)\varepsilon(E',E_c,\theta')T(E')\Big(1 \pm \Big[-\frac{v}{c}P_{\pm}A\cos\theta\Big]\Big)B(E)P(\theta,\theta',E,E')$$

$$\times dE'dEd\Omega_{\beta}d\Omega_{\gamma}dV\Big)$$

where ± refers to the polarization of the ^{35}Ar and the first term is detection of a positron emitted directly into the detector, while the second term is detection of a backscattered positron.

E = incident positron energy

E' = backscattered positron energy ~E/2 (see backscatter papers in references)

E_c = cut-off energy: this is a software cut performed on the energy spectrum

v = positron velocity

$P_{\pm}$ = polarization of $^{35}Ar \cong 6\%$ (≥ 0 by definition)

A = beta decay asymmetry parameter

f(E) = Fermi integrand: the energy distribution of positrons including the Coulomb correction

θ = polar angle of the incident positron $\leq 90°$ (the z axis is parallel to the axis of symmetry for the top and bottom plastic detectors)

θ' = polar angle of backscattered positron $\leq 90°$ (after backscattering)

$P(\theta',\theta,E,E')$ = the energy and angular distribution of backscattered positrons $\propto$ $E'(E-E')\cos^2(\theta'-[\pi-\theta])$, $\theta \geq 90°$ for backscattering positrons

B(E) = backscatter coefficient, i.e. the fraction of incident positrons that are backscattered from a material, ~2% for saturation backscatter from carbon

T(E) = the transmission coefficient for positrons of energy E to pass through the mylar foil and ΔE-detector. Transmission through the mylar is ~100% for the energy cuts used, but is decreased due to the ΔE-detector at the lower energies ($\leq$ 1.5 MeV). Transmission for the backscattered positrons must also include the transmission through additional material before backscattering toward the opposite detector.

$\epsilon(E,E_c)$ = efficiency to detect a positron with energy E with discrimination bias E_c.

To be exact, the energy should be reduced by the amount lost in the ΔE-detector. The efficiency is essentially constant except near the edges of the detector where the positron can escape before depositing an energy above the cut-off.

$d\Omega_\beta$ = solid angle element of the plastic detector. For the second term, this is symbolic of an integral over the "backward" solid angle and the solid angle, after backscattering, to enter the detector. I neglect the undetected backscatter out of the detector, which will not affect the asymmetry calculated for the detector from P_+ and P_- data since this backscattering positron has the same incident angular distribution as those detected.

$d\Omega_\gamma$ = solid angle element of the germanium detectors

dV = target cell volume element containing gas

$C_\pm$ = intrinsic ^{35}Ar activity, depending on the target cell pressure, beam energy, beam current, etc.

The backscatter term is small compared to the first term and can be dropped from the calculation. (What is really important is not the backscatter correction but the differential correction between β_0 and β_1.) Then the counts for a given cycle are given by,

$$N_{\pm} = C_{\pm}(I + JAP_{\pm})$$

where I and J are the energy + angular + volume integrals,

$$I = \int dE d\Omega_{\beta} dV d\Omega_{\gamma} f(E)\varepsilon T \ , \ J = \int dE d\Omega_{\beta} dV d\Omega_{\gamma} f(E)\varepsilon T \frac{v}{c}\cos\theta$$

If we denote the top detector by subscript 1 and the bottom detector by subscript 2 and collect for N cycles,

$$\Delta_T = \frac{N_{1+}-N_{1-}}{N_{1+}+N_{1-}} = \frac{I_1\sum_{i=1}^{N}(C_+-C_-)_i + J_1A\sum_{i=1}^{N}(C_+P_+ + C_-P_-)_i}{I_1\sum_{i=1}^{N}(C_++C_-)_i + J_1A\sum_{i=1}^{N}(C_+P_+ - C_-P_-)_i} \equiv \frac{\alpha+G_1A\beta}{\gamma+G_1A\delta}$$

similarly,

$$\Delta_B = \frac{N_{2+}-N_{2-}}{N_{2+}+N_{2-}} = \frac{\alpha-G_2A\beta}{\gamma-G_2A\delta}$$

where $G \equiv J/I$, $\gamma \equiv \Sigma(C_+ + C_-)_i$, $\alpha \equiv \Sigma(C_+ - C_-)_i$, $\beta \equiv \Sigma(C_+P_+ + C_-P_-)_i$, and $\delta \equiv \Sigma(C_+P_+ - C_-P_-)_i$. We have assumed the beam does not move spatially, causing a change in the geometry integrals I and J. The burns on the mylar entrance and exit foils verify that the beam was localized. Small drifts can be absorbed by the individual C's, in which case I and J represent the average geometry integrals. The analysis follows similar lines as presented here.

α,β, and δ are small compared to γ:

From the raw data for β_0 it is found that $\Delta C/C \sim 0.1\%$. A conservative estimate for $\Delta C/C$ from subrun to subrun is ~ 1%. The polarization, also determined from the data, is small: P ~ 6%. Using these values we find:

$\alpha \sim (\Delta C/C)\gamma \sim 1\%\gamma \quad \beta \sim P\gamma \sim 6\%\gamma \quad \delta \sim P\alpha \sim .06\%\gamma$

Finally the asymmetry Δ is calculated, correct to O(1%),

$$\Delta \equiv \Delta_T - \Delta_B \equiv \frac{(G_1+G_2)A\beta}{\gamma} = (G_1+G_2)A\frac{\sum_i (C_+P_+ + C_-P_-)_i}{\sum_i (C_+ + C_-)_i}$$

$$\equiv GAP$$

C. Calibration of Detectors

(a) HPGe

Calibration of the Ge detectors was performed with a ^{60}Co source (1173.2 & 1332.5 keV). As can be seen in figures 1c and 1d at the end this section, the gamma spectrum is very clean. The only significant lines are identified as the 511 keV annihilation gamma ray, the 511+511=1022 keV sum peak, the 1219.4 keV first excited-state decay of ^{35}Cl, the 1763.2 keV second excited-state decay of ^{35}Cl, and two "satellite" peaks above and below the 511 line identified as the 340 keV backscatter peak and the 511+171=682 kev backscattered photon sum peak.

As mentioned before, the Ge detectors had suffered neutron irradiation damage and had poorer resolution at higher energies as a result. The FWHM at 1219 keV was approximately 3 keV for both detectors, compared with 2 keV before the damaging run. The 511 keV line also suffered a reduction in resolution, but most of the broadening is due to the velocity smear of the positrons before annihilation.

(b) Plastic

The beta detectors were calibrated with a ^{207}Bi monoenergetic source, with MeV electron energies at 0.481(e_K)/0.554(e_L) and 0.976(e_K)/1.048(e_L), and a ^{106}Rh source with beta endpoint energy 3.54 MeV. Because of additional energy losses in passing through the mylar window and ΔE-detector for low energy positrons, the low energy end of the beta spectrum is nonlinear and difficult to calibrate. A consistency check can be performed with the ^{106}Rh source on the two β spectra, β_0 and β_1, associated with the 511 keV gamma ray and the 1219 keV gamma ray, respectively. Assuming the endpoint of the β_0 spectrum is T=4.9 MeV, the endpoint for the β_1 spectrum is calculated to be 3.7 MeV, the same as the experimentally determined value, for the top detector. This procedure leads to a discrepancy for the bottom detector, but seems to be a problem associated with the Rhodium source for the following two reasons:

(i) The energy discrepancy is approximately 300 keV, the energy loss in the ΔE-detector. It is possible that the source was accidently placed between the E and ΔE-detectors instead of between the target cell and the ΔE-detector.

(ii) The channel separation between β_0 and β_1 is the same for both detectors with a relative displacement of approximately 20 channels; this is significant because the gains of the systems were almost identical, so the separation would be expected to be the same. The ^{207}Bi tail plotted on a semi-log scale allows an "endpoint" to be determined fairly precisely even though the energy peaks are below the detector hardware cut-off. From this data, the ratio of the ^{207}Bi-β_0 channel separation to the β_1-β_0 channel separation can be compared for the two detectors, independent of gain. The ratio is identical for both detectors while for the ratio of ^{106}Rh-β_0 to β_1-β_0 there is a large discrepancy between top and bottom detectors. This implies that the relative endpoint positions of ^{207}Bi, β_0, and β_1 are all consistent for the two detectors while the endpoint of ^{106}Rh relative to ^{207}Bi, β_0, and β_1 is in disagreement for the top and bottom detectors.

While the calibration is crude, it must be emphasized that the 1219 keV gamma ray (and indirectly the 1763 keV) is unquestionable evidence for the first

excited-state positron's presence and it is with respect to this endpoint that the Rhodium endpoint is in discrepancy- the Rhodium endpoint is below the β_1 endpoint for the top detector, but above the β_1 endpoint for the bottom detector. The evidence implicates Rhodium (and a tired experimenter) beyond any serious doubt.

It can be seen that the endpoint of the β_0 spectrum is distorted (see Fig.1a), probably due to cosmic ray muons. The activity for muons in random coincidence with 511 keV activity generated from ^{13}N (estimated activity ~20-50× ^{35}Ar) agrees with what is expected. The energy deposition, taking into account the need to avoid the opposite detector veto and the angular distribution ~ $\cos^2\theta$ to the vertical, is predominantly between 4.5-5.5 MeV which is where the distortion is observed to occur. Two additional pieces of information required to arrive at this result are (1) an energy loss of 1.7 MeV/cm and (2) a light efficiency conversion of ~1.1%, compared with ~1.9% for positrons in pilot-B.[1]

Sample spectra from the run are shown in Figures 1a-1m. Figs. 1a,b show partial data for the top E-detector beta spectrum in coincidence with a 511 keV gamma ray and in coincidence with a 1219 keV gamma ray. Figure 1c is a linear scale plot above ~1 MeV from subrun #6 for the "right" Germanium detector (left and right is relative to the beampipe, looking into the incident beam). The

spectrum shows how prominent the 1219.4 keV line is compared to the other lines. (The small unidentified line on the right at 1293 keV is background from ^{58}Fe.) The shoulder on the low energy side of the peaks is characteristic of radiation damaged detectors. Also prominent in the spectrum is the 1763.2 keV line for the ^{35}Ar decay to the second excited state of ^{35}Cl (see Fig.1, chapter 2). The ratio of full energy counts for the two lines should be equal to the ratio of the intrinsic peak efficiencies multiplied by the corresponding branching ratios. The peak efficiency is approximately proportional to E^{-1} so $\beta_1/\beta_2 \approx (1763/1219)\times(0.0127/0.0023) \cong 8.0$. The observed ratio for a sample of the data (Ge right, subrun #6) is $\beta_1/\beta_2 \cong 2042/252 = 8.1\pm0.5$ in excellent agreement. The background of the 1219 line is approximately 10% and is dominated by annihilation-in-flight gamma rays from β_0 into the 1219 window. See section (g) for more details. Figure 1d shows the entire gamma spectum.

Figures 1e and 1f are the Rhodium and Bismuth calibration spectra, respectively. The energy peaks from the decay of Bismuth are not discernable and what is actually observed is the high energy tail of its ~1MeV monoenergetic electron, as well as the high energy cosmic ray muons in the upper channels of the spectrum. Although the energy corresponding to 1 MeV should lie above the hardware cut-off at the low end (approximately channel 30), it falls below the

cut-off because of the ΔE-detector. For beta radiation above about 2 MeV, the energy deposition in the ΔE-detector is approximately 300 keV. As the initial kinetic energy is lowered, the deposition increases, resulting in a nonlinear response in the main detector energy spectra versus channel number. Even though the hardware cut-off corresponds to approximately 0.4 MeV, based on high energy calibrations, the 1 MeV electrons lose more than 0.6 MeV in passing through the thin plastic. Figures 1g and 1h show the ΔE spectra for ^{207}Bi and ^{35}Ar; it is clear that for the lower energy Bismuth beta radiation, the energy loss is more severe than for the much higher average energy of the Argon spectrum. Not only is the ΔE peak for the Bismuth shifted to higher deposition energies, but the FWHM is about 40% larger.

Figures 1i-k show the β_0, β_1, and Rhodium spectrum for the top detector and reveal the relative positions of the endpoint energies.

Finally, Figures 1l and 1m show the TAC spectra for the top plastic in coincidence with the right Germanium (l) and the left (m) 511 keV line. The distortion in the peaks is most probably due to the neutron damage the Germanium detectors suffered in a previous run. The most prominent distortion is the extensive slewing on the short time side of the peak. This distortion was not present in the run prior to that in which the damage occurred. Since energy collection is incomplete due to charge trapping, it is possible that the gamma

signal is skewed in time toward longer times. Since the gamma signal starts the TAC, this means a shorter time separation between the gamma and positron signals. Thus the shoulder would be expected on the low side of the timing peak, as is observed. These shoulders, after background subtraction, represent approximately 30% of the TAC peak left and 13% of the TAC peak right. This is consistent with the left Ge suffering more damage than the right: FWHM at 511 keV is 3.8 keV for the left and 3.1 keV for the right. The background (above the coincidence peak) is approximately 5% for the left and 3.7% for the right (3.9% and 3.3% if the skewed shoulder below is folded into the counts of the coincidence peak); it is well accounted for by the ^{35}Ar activity and ^{13}N activity, producing 511 keV gammas from positron annihilation in the target walls and plastic absorbers in front of the Ge detectors. See section (g) for details.

The difference in counts between the two germanium detectors for 511 keV gamma rays, manifested in the difference in counts between the two TAC spectra, is due to the right germanium detector being closer to the positron detectors from where the 511 keV gamma rays originate as well as to having less 511 keV gamma rays in the low energy shoulder of the 511 keV spectrum (due to the damage the detectors suffered) and more in the gated peak. (For the 1219 keV gamma rays, originating in the target cell from which both gamma detectors are equidistant, the counts are the same for the two detectors as would be expected.)

Figures 1:

Figure 1a: Positron spectrum obtained in coincidence with 511 keV gamma rays. This spectrum consists of data obtained with both beta detectors for 10 hours collection time.

Figure 1b: Positron spectrum obtained in coincidence with 1219 keV gamma rays, consisting of positrons associated with ^{35}Ar decay to the first excited state of ^{35}Cl. This spectrum represents ~ 40 hours of data collection using both detectors.

Figure 1c: Gamma ray spectrum above ~1MeV. This spectrum consists of data obtained with a single Ge detector for 10 hours collection time.

Figure 1d: Semi-log plot of complete gamma ray energy spectrum for 1c above.

Figure 1e: Electron spectrum of ^{106}Rh.

Figure 1f: Monoenergetic electron spectrum of ^{207}Bi.

Figure 1g: ΔE-detector spectrum of ^{207}Bi.

Figure 1h: ΔE-detector spectrum of ^{35}Ar.

Figure 1i-1k: ^{106}Rh spectrum (i) and ^{35}Ar positron spectrum for the top detector in coincidence with a 1219 keV (j) and 511 keV (k) gamma ray emphasizing the relative positions of the endpoints.

Figure 1l,1m: TAC coincidence timing spectra between a top detector positron and a 511 keV gamma ray in the right (l) and left (m) germanium detectors.

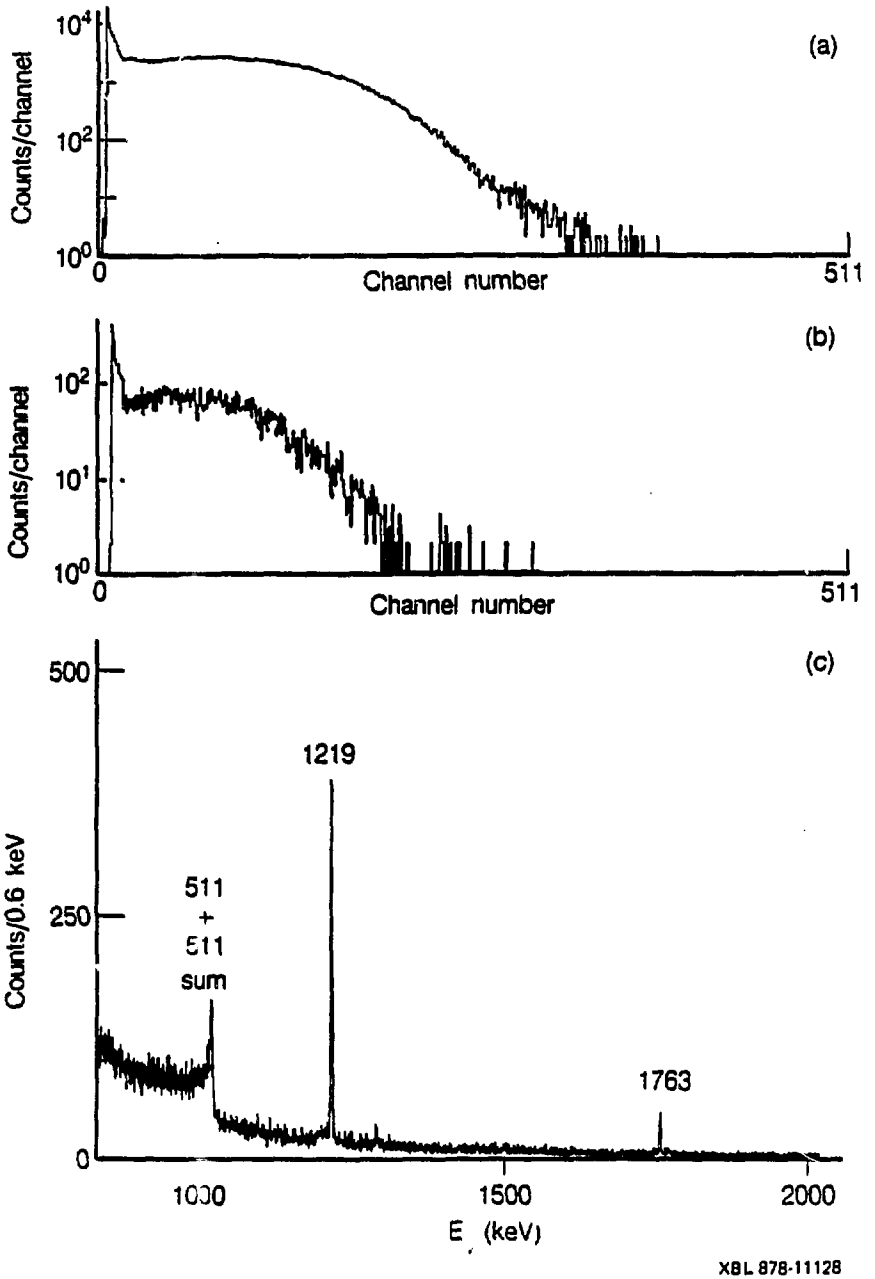
(a)
Counts/channel
10^4
10^2
10^0
0
Channel number
511
(b)
Counts/channel
10^2
10^1
10^0
0
Channel number
511
(c)
Counts/0.6 keV
500
250
0
1219
511
+
511
sum
1763
1000
1500
2000
E (keV)
XBL 878-11128

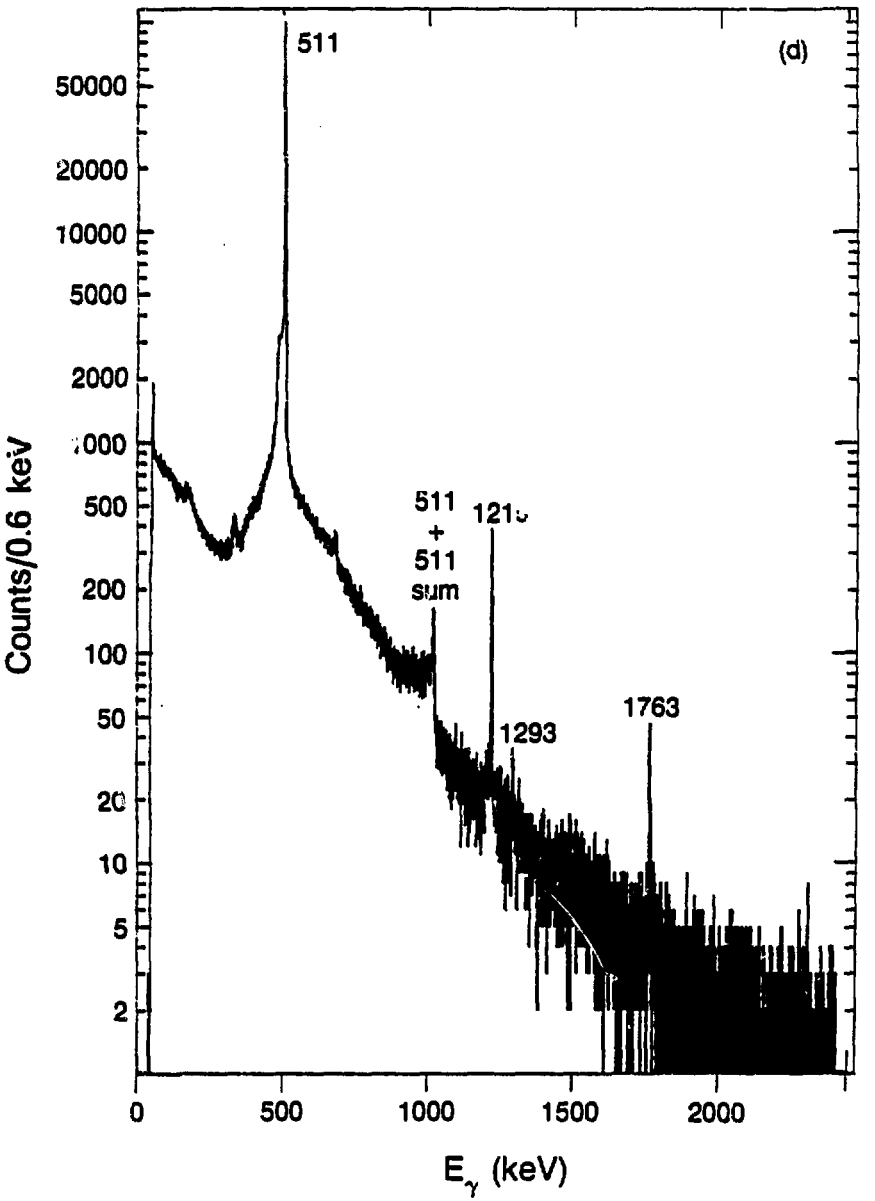

XBL 8710-5920

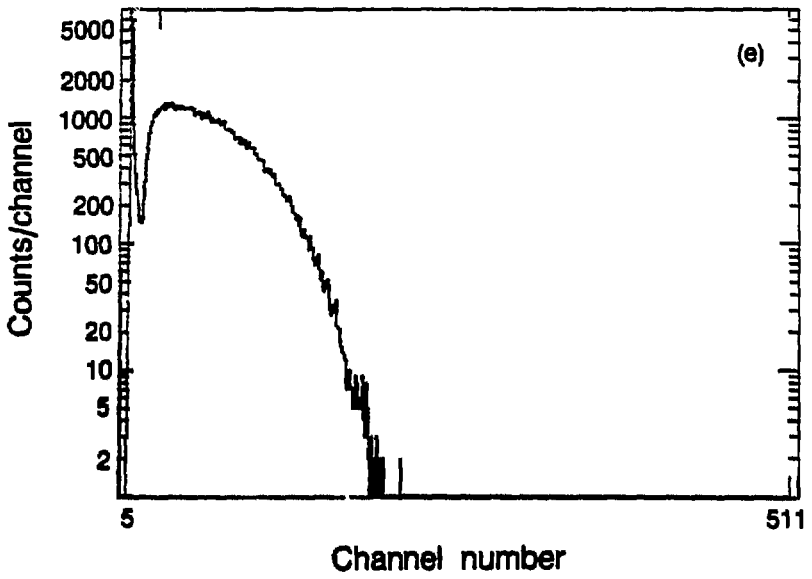

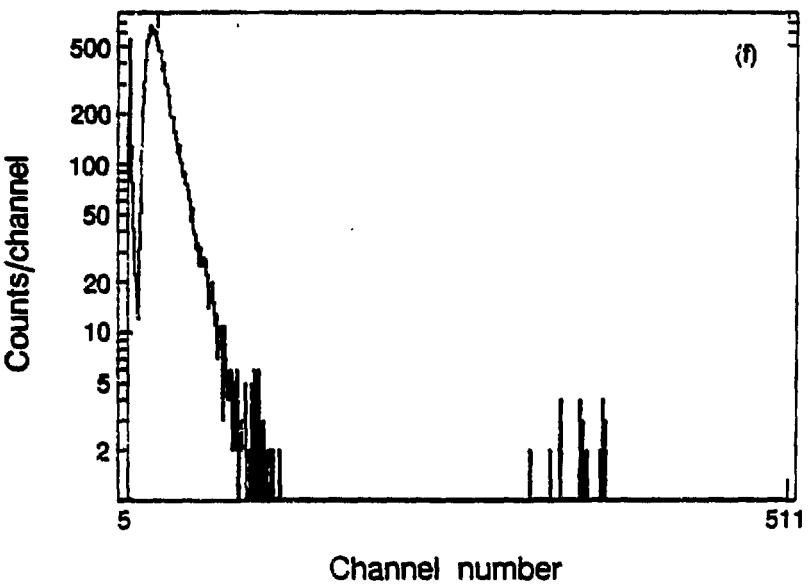

XBL 8710-5918

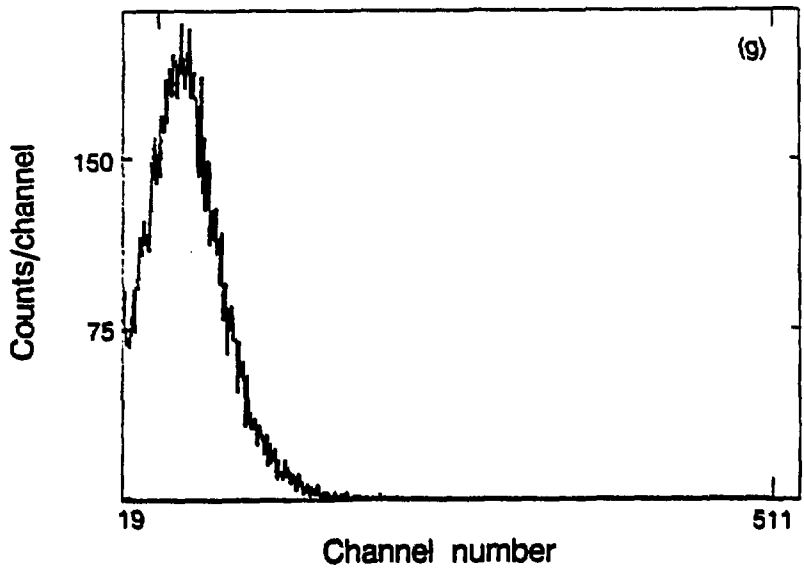

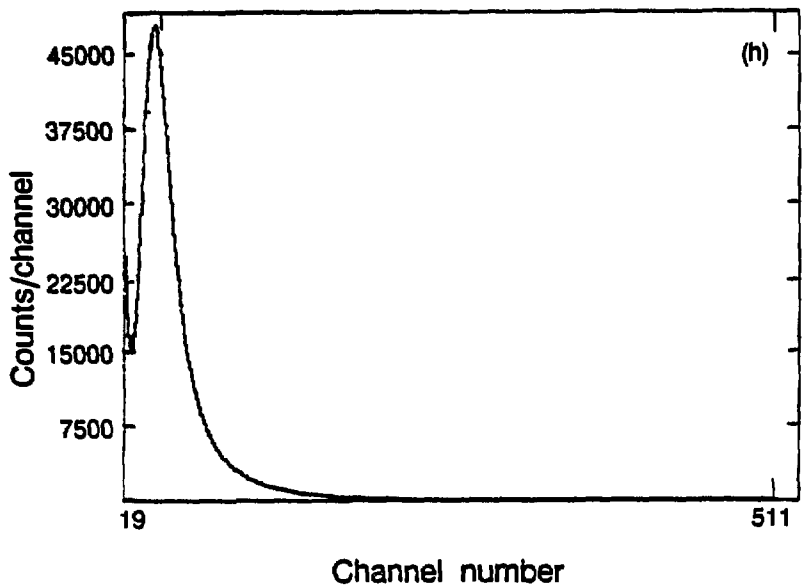

XBL 8710-5922

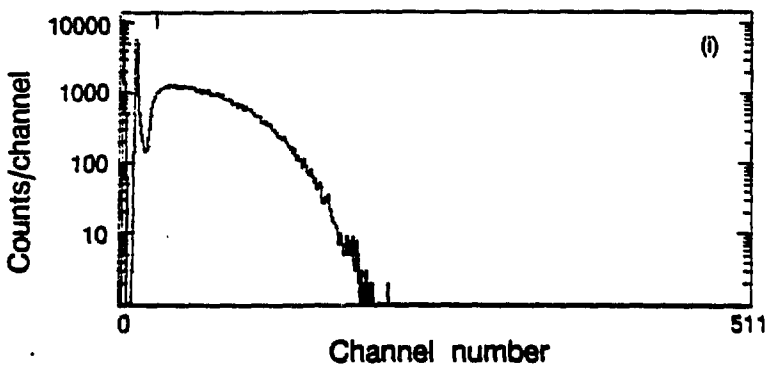

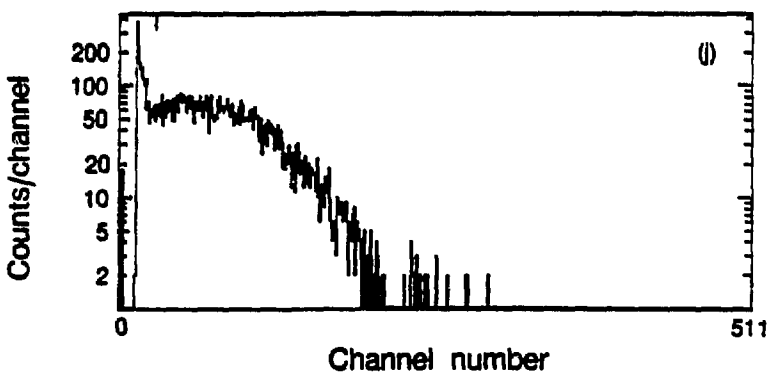

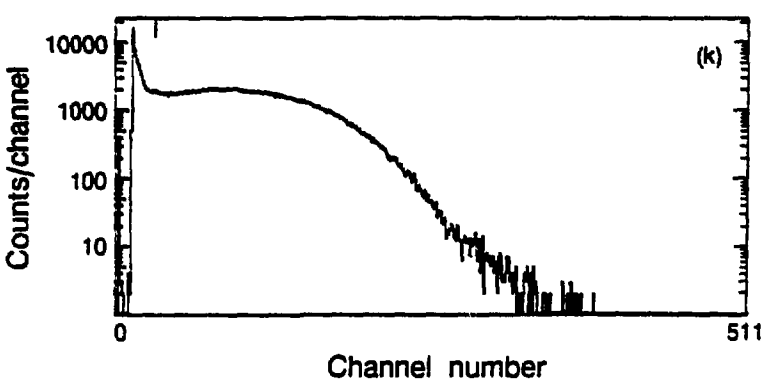

XBL 8710-5921

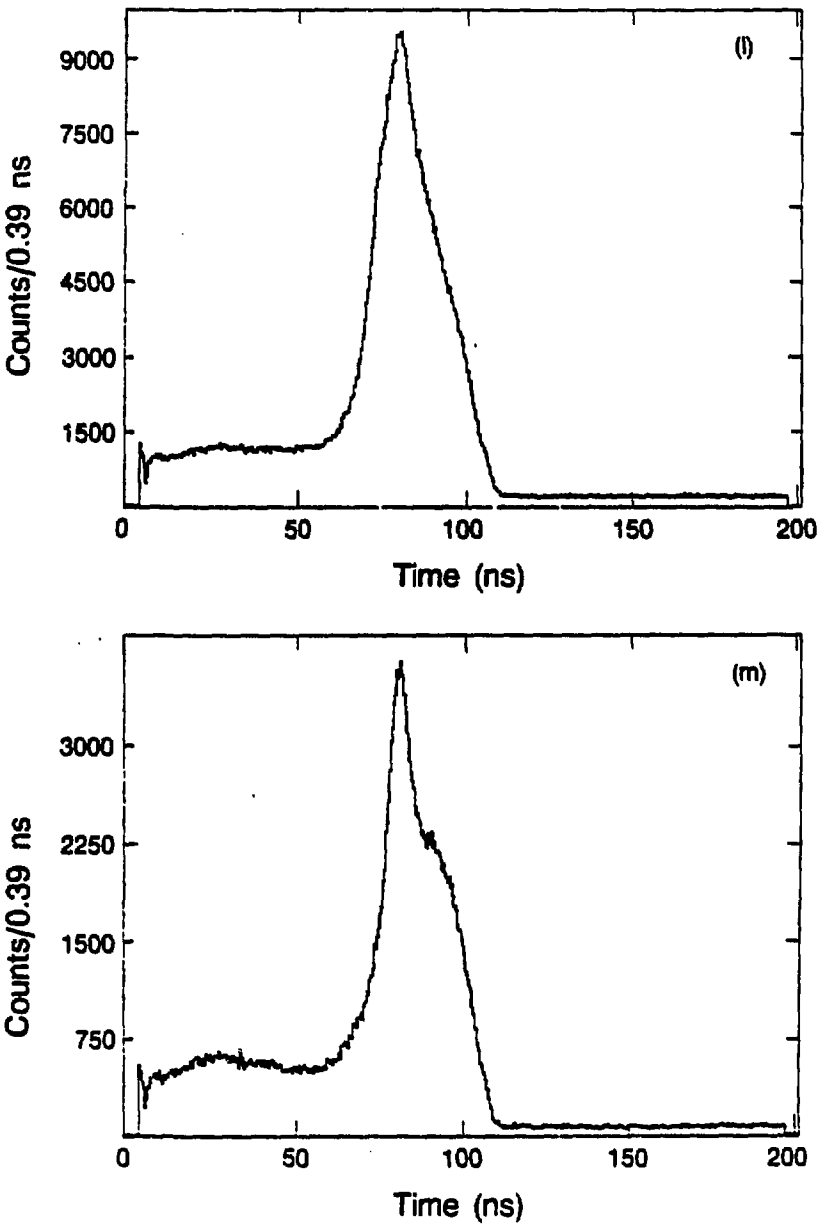

XBL 8710-5919

D. Cuts on the Data

The asymmetry is calculated from the counts in the beta spectra, spectra numbers 2 and 4 (see Table 1a). Various energy cuts and gates are imposed on the spectra to extract the cleanest data. These selection criteria are tabulated in Table 2 below:

Table 2: final gate selections

gates on positron spectra	selection
P_+, 511 peak, TAC peak	β_0 with 511 coincidence
P_-, 511 peak, TAC peak	β_0 with 511 coincidence
P_+, 1219 peak, TAC peak	β_1 with 1219 coincidence
P_-, 1219 peak, TAC peak	β_1 with 1219 coincidence
P_+, above 1219, TAC peak	β_1 background correction
P_-, above 1219, TAC peak	β_1 background correction
P_+, below 1219, TAC peak	β_1 background correction
P_-, below 1219, TAC peak	β_1 background correction

The positron associated with ^{35}Ar decay to the first excited state of ^{35}Cl is extracted from the beta spectra by a prompt coincidence requirement with a 1219 keV gamma ray. The background of the gamma spectra is dominated by annihilation-in-flight gamma rays from β_0 in the main plastic detectors. Because this will produce a prompt β-γ coincidence, the narrow TAC gate on the timing peak will not remove this contribution.Since the background is approximately 10%, it is not negligible and must be subtracted by interpolation of data obtained by gating with a gamma energy window above and below the 1219 keV window.

The β_0 (plus a small β_1 contribution) spectrum is obtained by a coincidence requirement with a 511 keV annihilation gamma ray. Positrons coming to rest in the plastic detectors will annihilate producing a prompt coincidence. Our decision to determine the groundstate asymmetry by this coincidence measurement rather than just using "singles" data is based on three compelling reasons:

(i) It suppresses noise and gamma rays in the beta spectrum (as does the ΔE-E telescope) and will also suppress detection of electron decays, if any are present.
(ii) Since a beta signal that is associated with a TAC must be a valid signal (see chapter 2B.b), it removes invalid beta signals that are recorded because they randomly arrive at the AtoD converter within the 2 μsec window opened after a master gate signal is generated from a valid signal from the opposite detector system.
(iii) The coincidence requirement results in a geometry factor G_0 that is calculated analogously to G_1. Although the factors will not be identical since the β_0 annihilation 511 keV gamma rays are produced inside the plastic detector and not inside the target volume, they are more similar than the singles geometry factor. See section (g) for more details on the geometry correction.

The end result of the coincidence requirement is much cleaner data at a

slight cost in statistics. (This cost was not significant since the β_1 data sample is smaller by a factor of ~100 compared to that of β_0 coincidence data.) Earlier studies of the data used different selection criteria than those listed in Table 2. Some of that data is presented in the following sections; it was used for stability checks and reproducibility checks, but was not used in the final asymmetry calculation.

E. Energy Dependence of Δ

The energy dependence of Δ_T or Δ_B is manifested in the geometry factor G:

$$G = \frac{\int [f(E)\varepsilon T \frac{v}{c}\cos\theta] dE d\Omega_\beta d\Omega_\gamma dV}{\int [f(E)\varepsilon T] dE d\Omega_\beta d\Omega_\gamma dV}$$

G can be considered an average of (v/c)cosθ, weighted by the distribution f(E)εT. The value of this average is a function of the energy limits of the integration. The quantity v/c varies by ~6% between 1 MeV and 5MeV (kinetic energy), and cosθ varies as a function of energy because the detector efficiency drops near the edges of the detector for higher energy positrons. Both effects tend to increase the geometry factor with increasing upper integration energy limit, but overall these effects are mild and G will not vary by more than a few percent from some

average value.

Figures 2a&b present plots of the asymmetry as a function of channel bins, either ten or twenty channels per bin (the entire spectrum covers ~ 250 channels). This corresponds to binning the asymmetry by energy E with spread ΔE. The energy spanned is appproximately 1.2 MeV to 4.2 MeV with a spread of approximately 0.018 MeV/channel for the higher energy channels. From the plots, it is clear that the asymmetry is stable. This stability versus energy was observed for all the subruns; in addition, the asymmetry determined from real time data displayed during each subrun showed no deviation, within statistical fluctiations, as a function of time, often over several hours. A slow variation could be discerned over longer time periods; but the fluctuations in asymmetry between subruns was no more than 20% and was usually less than 12% (for the subruns after #602, representing 80% of all the data). This variation is attributed to drift in the polarization of the proton beam.

Figure 2a (next page): The asymmetry Δ for the top and bottom detectors as a function of energy. Each energy bin represents ~0.36 MeV spread (more for the lower channels) and the range is approximately 1.1 MeV to 4.2 MeV. These data are from subrun 603. It consists of betas in coincidence with a 511 keV gamma ray for the left Ge. The bin width is 20 channels.

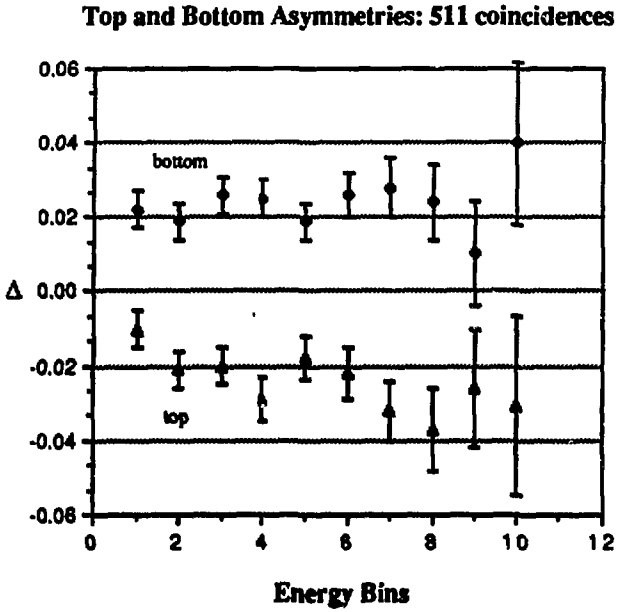

Figure 2b (next page): The asymmetry Δ for the top and bottom detectors as a function of energy. Each energy bin represents ~0.18 MeV spread and the range is approximately 1.1 MeV to 4.2 MeV. These data are from subrun 608. It consists of the raw beta spectrum gated only by the polarization. The bin width is 10 channels. The important point to be concluded here is that even the raw data is very stable as a function of energy and the asymmetry is the same, within statistical uncertainty, to the processed data shown in Figure 2a above.

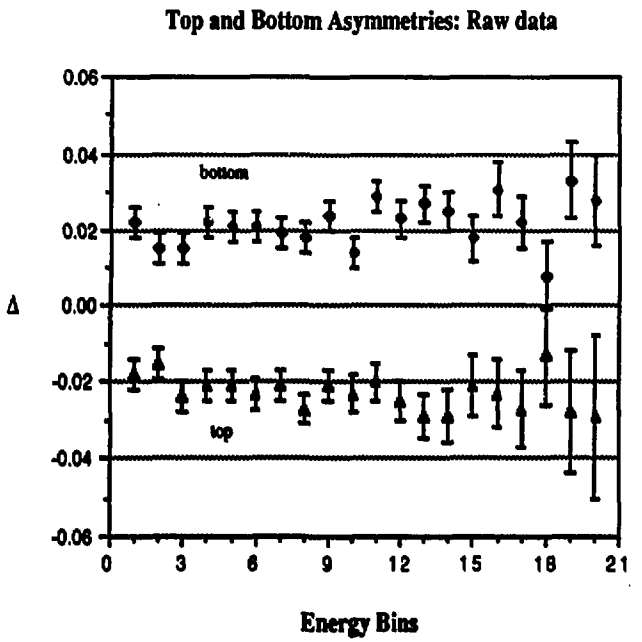

Figure 2c (next page): The aymmetry integrated over energy for the top and bottom detectors for each of the subruns. The beta spectra are taken in coincidence with a 511 keV gamma ray and all the final cuts listed in Table 1. These data are also tabulated below in Table 3. (The asymmetry for the top and bottom detectors in coincidence with a 1219 keV gamma ray for each subrun is tabulated in Table 3 below but because of the large uncertainties in the individual asymmetries, they are not presented in graphic form.)

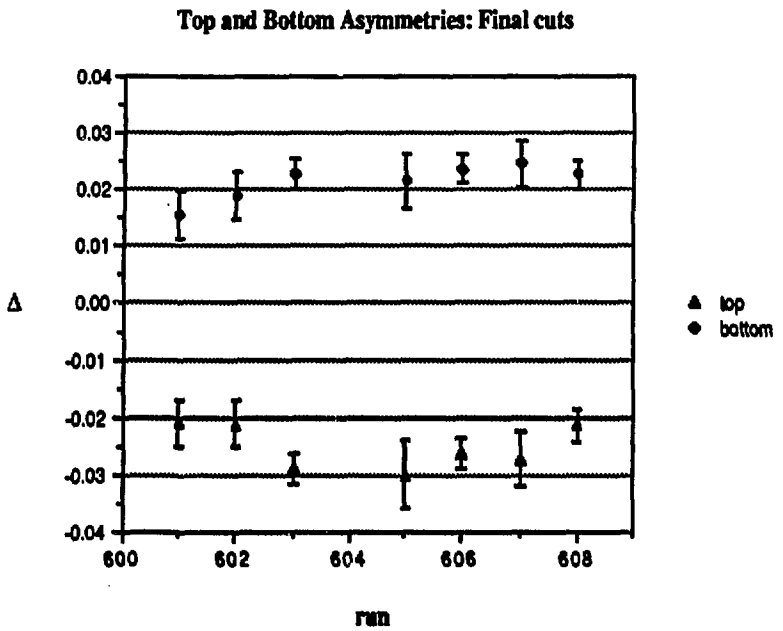

F. Gated Data and the Asymmetry

The asymmetry data are presented in Table 3. The data for β_0 had a low energy cut at channel 100, corresponding to an energy ≈1.7 MeV, and a high energy cut just below the muon distortion. The lower cut-off was chosen to lie well above the 1.2 MeV (kinetic) endpoint of ^{13}N. The β_1 data was cut at channel 30, just above the hardware cut-off. This channel lies above the low energy pile-up (see Figure 1a) and corresponds to an effective cut-off ≈1.1 MeV. The

annihilation-in-flight (1219±4.8) keV gamma rays from (mostly) β_0 are removed by subtraction of approximately 10% of the peak data, calculated by interpolation of data obtained from 9.6 keV windows located above and below the peak. The relative weights of the two windows are 0.73 for the window above and 0.27 for the window below. (The lower window was placed low enough to avoid contamination from the 1219 keV shoulder and 1173 keV ^{60}Co contamination line.)

Table 3: asymmetries

run #	Δ_{0top}	$\Delta_{0bottom}$	Δ_{1top}	$\Delta_{1bottom}$
601	-0.0210±0.0040	0.0155±0.0042	-0.0808±0.0391	-0.0168±0.0419
602	-0.0211±0.0039	0.0190±0.0043	-0.0107±0.0377	0.0608±0.0400
603	-0.0289±0.0028	0.0227±0.0026	-0.0543±0.0286	0.0043±0.0265
605	-0.0299±0.0060	0.0215±0.0047	-0.1223±0.0679	0.0846±0.0565
606	-0.0262±0.0027	0.0237±0.0024	-0.0825±0.0271	0.0562±0.0255
607	-0.0272±0.0048	0.0245±0.0041	-0.0521±0.0470	0.0749±0.0429
608	-0.0214±0.0030	0.0226±0.0026	-0.0119±0.0296	0.0483±0.0271

The average of these runs is obtained by maximum likelihood, i.e. the individual subruns are weighted by the inverse of the square of their quoted uncertainty. This represents a weighting of each run by its total counts in a given detector. The results are:

$$\Delta_{0top} = -0.0245 \pm 0.0013 \qquad \Delta_{0bottom} = 0.0221 \pm 0.0012$$

$$\Delta_{1top} = -0.0526 \pm 0.0132 \qquad \Delta_{1bottom} = 0.0398 \pm 0.0125$$

$$\frac{\Delta_{0top} - \Delta_{0bottom}}{\Delta_{1top} - \Delta_{1bottom}} = 0.504 \pm 0.101$$

G. Corrections

This section describes the corrections for the systematics to the above result. All the corrections are small so it is unnecessary to rely on the full expression for Δ (see section A) in order to introduce the corrections properly. To lowest order, the corrections enter simply as multiplicative factors except for the effective branching ratio correction.

(a) Deadtime correction

The deadtime for each detector system ranged between ~2-8%, depending on the subrun. This does not include the computer deadtime of 2μsec per event that was common to every channel. To lowest order, the deadtime correction to Δ_0 or Δ_1 is the difference in deadtimes between the top and bottom detector systems, which is ≤1%. The ratio Δ_0/Δ_1 cancels this deadtime correction to lowest order. At most, the correction is ≤0.2%, which is negligible.

(b) Effective branching ratios

The "β_0" spectrum is not entirely due to ^{35}Ar decay to the groundstate of ^{35}Cl, but rather, is a mixture of all the excited state transitions and the groundstate transition. The asymmetry for "β_0" is obtained from a low energy cut at ~1.6-1.8 MeV which will weigh the groundstate more heavily than by the simple ratio of branching ratios since the excited spectra will have a greater fraction of their spectra removed by the cut-off. The correction enters as follows:

$$\Delta_{0\text{experimental}} \cong (1-\frac{f_1+f_2}{f_0})(\Delta_0+\frac{f_1}{f_0}\Delta_1+\frac{f_2}{f_0}\Delta_2)$$

where f denotes the branching ratio and the subscript labels the branch. It must be remembered that all the Δ's in this expression are obtained from an energy cut above channel 100. Thus the ratio of this expression with Δ_1 obtained by coincidence with a 1219 keV gamma ray must take into account the different value for the geometry factor at the different energy cut, due primarily to the (v/c) effect. The second excited-state branch f_2 is small compared to f_1.

Taking the known branching ratios and integrating the (allowed) energy distributions with lower cut-offs ranging from 1.4 MeV to 2.0 MeV, a spread of effective branching ratios is obtained. The calculation neglects the Coulomb correction, which should be small and negligible compared to the estimated uncertainty. Only the first and second excited state decays contribute

significantly. The correction is:

$$\frac{f_1}{f_0} = 0.009 \pm 0.001, \quad \frac{f_2}{f_0} = 0.0012 \pm 0.0005$$

$$\frac{f_1 + f_2}{f_0} = (1.0 \pm 0.2) \times 10^{-2}$$

The correction tends to decrease the ratio Δ_0/Δ_1 .

(c) Background correction

The background was monitored by runs without CCl_4 in the target cell. It had no asymmetry and was a approximately 4% of the signal. The background was due to CCl_4 which leaked into the beampipes, and to ^{13}N produced by a (p,n) reaction on ^{13}C in the mylar entrance and exit foils and in the CCl_4. The ^{13}N doesn't enter into the asymmetry for a simple reason: its endpoint energy for positron decay is T=1.2 MeV, so it is not detected directly in the plastics. It can be detected by annihilation of the ^{13}N positron in a ΔE-detector with emission of a 511 keV gamma ray into the main plastic, which has a detection efficiency ~10%. However this low energy signal is removed from the Δ_0 calculation by the ~1.7 MeV energy cut, and does not contribute to Δ_1, since it only occurs in random coincidence with a 1219 keV gamma ray, which is negligible at the observed beta activity.

The dominant background was due to ^{35}Ar in the beampipes near the mylar windows. The 1219 keV activity detected was consistent with this hypothesis, albeit with a large uncertainty due to the very few counts (<10). Because the asymmetry was consistent with zero, determined from the β_0 spectrum, the background reduces the measured asymmetry Δ. If the activity were all ^{35}Ar, then the background factors for Δ_0 and Δ_1 would be the same, up to geometry factors, and cancel in the ratio. To be conservative we choose a correction factor:

$$\frac{B_0}{B_1} = \frac{1+\frac{N_{B1}}{N_1}}{1+\frac{N_{B0}}{N_0}} = 1.02 \pm 0.03$$

The correction increases the ratio Δ_0 / Δ_1.

(d) Random coincidence correction

Random coincidence in β_1 is dominated by β_0 annihilation-in-flight gamma rays in random coincidence with β_0. This event is enhanced by β_0's that pass through the target walls and annihilate in the plastic absorbers directly in front of the Germanium detectors, greatly increasing the gamma solid angle ~x5-10; additionally, there is an enhancement due to positron momentum in the

direction of the Ge detectors, which defines a preferred cone of emission for the annihilation-in-flight gammas. This random coincidence is also present in the beta spectra generated with an energy window above or below the 1219 keV gamma line, so the background subtraction performed on the β_1 data already corrects for it.

Random coincidence in β_0 will also have a contribution from β_0 annihilation near the Germanium detectors in random coincidence with β_0. It will also have a large contribution due to β_0 in random coincidence with the ^{13}N 511 keV activity. This is estimated to be ~20× β_0 activity; nevertheless, this background carries the asymmetry Δ_0 and produces no correction to Δ_0. Looking at the asymmetry in the upper channels of the TAC spectra (only due to random coincidence) verifies this assumption, i.e. the random coincidences carry an asymmetry consistent with Δ_T and Δ_B.

(e) Backscatter correction

The experiment was carefully designed to minimize backscatter. The interaction region is surrounded by plastic. Saturation backscatter from carbon at normal incidence is ≤2%[2] above ~1 MeV. The correction to the ratio Δ_0/Δ_1 is

even smaller, since it involves the change in backscattering for β_0 versus β_1.

Saturation backscattering occurs at material thicknesses ~0.2R, where R is the practical range of the beta radiation in the material. This is understood qualitatively by the following argument: beta radiation penetrating deeper than R/2 will never come back out of the material because of energy losses, so there is a play-off between increasing the probability to backscatter by penetrating deeper and not penetrating so deeply that it is not possible to escape. In other words, backscattering is zero for zero thickness and zero for positrons backscattered from a depth greater than R/2- it must peak somewhere between these values. So saturation backscatter will be reached at some thickness between 0 and R/2. A first guess would be ~R/4.

It is important to distinguish between the practical range, defined as the mean depth of penetration of a particle in a material, and the "continuous slowing down approximation range", used previously in this thesis, which is the total integrated path length until the particle comes to rest.[3] The practical range is a more useful experimental parameter, since it folds in the fact that beta particles do not travel in a straight line as they pass through materials.

The practical range for electrons is given by the empirical equation[4] (sufficient for our purposes):

$$R_{extrapolated}[\frac{g}{cm^2}] = 0.565(\frac{125}{Z_{effective}+112})E[MeV]-0.423(\frac{175}{Z_{eff}+162})$$

where Z_{eff} = 5.3 for pilot-B. The practical ("extrapolated") range at T=1 MeV is R_{ex}=0.47 g/cm^2=0.45cm for pilot-B. It rises to 1.0cm at 2.0 MeV, 2.0cm at 3.5 MeV, and 3.0cm at 5.9 MeV. For comparison, the thickness of the ΔE-detector is 0.16cm (not including the tape wrapping) and the thickness of the main detectors is 3.8cm.

Backscatter from the opposite detector system is highly suppressed when the energy losses and energy cuts imposed on the data are considered. The average backscattered energy is $<T_{incident}/2$, and drops rapidly with increasing incident energy (deeper penetration) and lower Z of the material.[5] This results in severe constraints on backscatter from the opposit E-detector: the backscattered positron will lose ~T/2 plus ~700 keV in passing back through the ΔE-detector and mylar foils and must then deposit enough energy in the E-detector to be detected, but <u>not</u> have deposited enough energy in the opposite E-detector to allow a veto. The veto will occur for an energy deposition lower than the cut-offs imposed on the data for "detection", depending only on the much lower hardware cut-off. This is an insurmountable constraint and effectively rules out this scenario for backscatter.

Backscatter from the oppposite ΔE-detector has the advantage of no veto, but the disadvantage of not occuring in the saturation region. To be detected

above a 1 MeV cut-off the incident positron must have >2 MeV kinetic energy. At this energy, the backscatter coefficient η is already falling below saturation. The backscattering is approximated by the empirical relation[4],

$$\frac{\eta(t)}{\eta_{sat}} = 1-e^{-(2t/t_{1/2})^2}$$

where t=material thickness=0.18g/cm^2 for the ΔE-detector, and $t_{1/2}\cong 0.28T^{1.21}$ [g/cm^2] for pilot-B is the thickness at which transmission is down by 50%. For T~3 MeV positrons, $\eta\cong 10\%\eta_{sat}$ which is negligible.

Backscattering is dominated by backscatter from the target walls. The wall thickness is 0.8cm. At T=5 MeV, $\eta\cong 60\%\eta_{sat}$ so for most of the energy spectrum the backscatter is close to saturation. Using the empirical backscatter coefficient of Kuzminikh and Vorobiev[6] for normal incidence and integrating over the positron energy spectrum above ~$2T_{cut\text{-}off}$ (normalized by the spectrum above $T_{cut\text{-}off}$ for direct incident positrons) we obtain a value for the correction. This is an upper limit (in the sense that it is a measure of the maximam deviation from unity) because from the K-V paper there is evidence presented that positron backscatter rises with increasing angle of incidence. Although we do not understand why this should occur, the effect is fairly insensitive to energy, so it

would lessen the change in backscatter between β_0 and β_1. In addition, the average energy of backscattered positrons from carbon is less than T/2, so the integration includes an excess of positrons available for backscatter- this effect tends to enhance the difference in backscatter between β_0 and β_1, and so offsets the effect mentioned above. Choosing a cut-off T_1=1.1 MeV and T_0=1.8 MeV a value for the correction is obtained:

$$\frac{1+2\eta_0}{1+2\eta_1} = 0.99 \pm 0.01$$

The factors of 2 come from the opposite asymmetry that the backscattered positrons carry, which enhances the effect when the asymmetry is calculated. The uncertainty is only an estimate. The correction decreases the ratio Δ_0/Δ_1.

(f) Geometry correction

Calculation of G (see sections B and E of this chapter) requires an eight dimensional integration. This was calculated using a Monte Carlo simulation, which took into account the positions of all detectors, the v/c effect, the attenuation factor for the gamma rays in the Ge detectors, the dead inner core of the Ge detectors, and the reduced detection efficiency of the betas at the edges of the scintillation detectors. The simulation was done with two diffusion models for ^{35}Ar in the He buffer gas, representing the two limiting cases for diffusion during

the counting period. The first was a distended line source located where the beam passed through the target, and the second was a uniform distribution inside the target cell. The true model lies somewhere between these two extremes. (An analytic solution for a delta function line source generated at t=0 sec can be obtained. For 1atm of He buffer gas, the ^{35}Ar diffuses quite slowly: only 10% of the initial ^{35}Ar diffuses outside a concentric cylinder, with 3cm radius, in the 3.2 sec counting period. This suggests the line source model is probably closest to the true diffusion pattern.)

The geometry factor is the ratio of two angular integrals; while the individual integrals varied by a few tens of percent, depending on the diffusion model, the ratio was fairly insensitive to these variations. This was even more the case for the ratio G_0/G_1. A conceptual description of the integration follows to provide a better understanding of the approach. This description is purely pedagogical, the Monte Carlo program disregarding a step by step approach to the integration:

A volume element is chosen and because the ΔE-detectors force acceptance only of those positrons that pass through the face of the main detector, the solid angle integration is limited to this face. This is integrated over the energy distribution of the positrons, f(E), and mildly weighted by the efficiency ε(E) which was assigned the value 1 if the chord of the straight line trajectory through the E-detector deposited the minimum cut-off energy; otherwise, it was assigned a value 0. This had the effect of reducing the detection efficiency of the

plastic for high energy positrons near the edges of the detector. For simplicity, the transmission was assumed to be 1 for the integrated energies. This is not true at the low energy end but since the variation is mild it could safely be ignored and monitored by seeing the effect on G by raising the cut-off energy. The effect was very small.

This beta integration is then weighted by the integration over the gamma ray solid angle. For G_0, this involved a gamma ray generated from where the beta particle penetrated the plastic and for G_1, it involved the target volume element. Separate integrations are performed over the faces of the Ge detectors and their sides. Except for geometrical effects, it is assumed that the intrinsic efficiency is the same for entrance into the Ge from the face or side.[7] A gamma ray's efficiency for detection is calculated by determining the chord through the Ge detector, discounting the inner dead core, and weighting the event by $(1-\exp[-\mu l])$, where "l" is the chord length and $\mu \cong 0.132 cm^{-1}$ for 1219 keV gammas is the attenuation length. This efficiency weighting has a very mild effect on G; again, it is the ratio of the integrals that is important and this minimizes the influence of the efficiency. The integration over the gamma ray detector solid angles has the effect of weighting the target volume elements differently. Because it is a ratio of integrals and because one gains back somewhat in solid angle on the edges of the detectors what one loses on the faces, this integration turns out to have a mild effect on the geometry factor.

One reason the β_0 data was selected by requiring a 511 keV coincidence was to make the geometry integrals as analogous as possible. One indication of how different G_0 and G_1 may be, is to look at the experimental geometry factors for β_0 singles (no coincidence with a gamma ray) versus β_0 coincidences with a 511 keV. This provides an extreme case, since one geometry factor is weighted by the Ge detectors while the other factor has no dependence on the germanium detectors. The result calculated is determined from runs 603, 606, and 608, the three biggest runs, and the coincidence data uses the final analysis cuts:

$$\left\langle \frac{\Delta_{0\text{singles}}}{\Delta_{0\text{coincidence}}} \right\rangle = \left\langle \frac{G_{0\text{sing}}}{G_{0\text{coinc}}} \right\rangle = 0.97 \pm 0.06$$

The Monte Carlo predicts (for the uniform distribution) 1.000±0.004. The experimental result implies that the geometry correction must be only a few percent. This is what is found with the simulation.

The Monte Carlo was tested by setting up artificial situations that could be solved analytically. All these tests give agreement to within 0.5% with the Monte Carlo and within the Monte Carlo estimated uncertainty. In addition, I integrated out one dimension and the new function, when evaluated with the Monte Carlo, gave the same answers. Solid angles extracted from the Monte Carlo data agree with analytic solutions for simple geometries and estimates for more difficult geometries involving the sides of the Ge detectors.

The Monte Carlo itself is a sophisticated program called VEGAS, written by G. P. Lepage. It divides the integration space up into hypercubes and with a random number generator, selects a point in each cube and evaluates the integral at this point. The program then iterates, shuffling the density of cubes to those regions that are changing most rapidly. Monitoring the variation from iteration to iteration provides information on the stability of the solution. The entire simulation was run on the Lawrence Berkeley Laboratory's VAX/VMS computer system.

The result turned out to be fairly insensitive to small changes in geometry and to the different diffusion models. The final result with my estimate of the uncertainty (based on the scatter in G_0/G_1 as a function of energy cut and diffusion model) is,

$$\frac{G_0}{G_1} = 1.02 \pm 0.02$$

The correction decreases the ratio Δ_0/Δ_1.

(g) Weak magnetism correction

For J_i , $J_f \geq 1$, differences in the alignment of the proton spin axis, for spin up versus down,with respect to the magnetic field can lead to a quadrupole moment in the angular distribution of positrons. This "weak magnetism" correction is a recoil effect and is smaller than the usual terms by a factor $\sim E_e/M_{nuclear}$, but may

not be negligible compared to AP for low polarization. The distribution is given by[9]:

$$dW \propto 1 + A\frac{\langle J_i \rangle \cdot p_e}{J_i E_e} + \frac{E_e}{2M_{nuc}}\left[\frac{\rho^2 + \rho N\left(\frac{J_i+1}{J_i}\right)^{1/2}\mu}{1+\rho^2}\right]\Lambda\left[\frac{p_e^2}{E_e^2}\cos^2\theta - \frac{p_e^2}{3E_e^2}\right]$$

where N=mass number=35, μ=the difference between the isovector contributions to the total magnetic moment, in units of μ_{proton}, between Argon-35 and Chlorine-35, $\rho = G_a\langle\sigma\rangle/G_v\langle 1\rangle$, and Λ is the "quadrupole moment" given by,

$$\Lambda = 1 - \frac{3\langle m_J^2 \rangle}{J_i(J_i+1)}$$

The polarization P is the "dipole moment",

$$P = \frac{\langle J_i \rangle}{J_i} = \frac{\langle m_J \rangle}{J_i}\hat{z} \cong \pm 0.06\hat{z}$$

Using $|\rho| \cong 0.3$ (for A_0=0.5, ρ=-0.28 and decreases in magnitude for decreasing A_0) and $\mu = [\mu(Cl) - \mu(Ar)]/[I_3(Cl) - I_3(Ar)] = -0.2nm = -0.07\ \mu_{proton}$,

$$dW \propto 1 + \frac{v}{c}PA\cos\theta + \frac{E_e}{2M_{nuc}}\Lambda\left[\left(\frac{v}{c}\right)^2\cos^2\theta - \frac{1}{3}\left(\frac{v}{c}\right)^2\right]$$

The value of P does not constrain Λ, and it is possible (although not probable) to

have $|\Lambda| \leq 1$. This produces the following orders of magnitude,

$$(v/c)PA \leq 0.06(0.5) = 0.03$$

$$(E_e/2M_{nuc})\Lambda \leq (5MeV)/(70GeV) \cong 7\times10^{-5}$$

Note that the third term in the expression for dW above is even under coordinate inversion. Thus it cannot contribute to the difference $(N_+ - N_-)$ except for differential misalignment of the incident proton spin. Thus we have:

$$\Delta_{top} = G_{top}AP + \frac{\langle E_e \rangle_{top}}{2M_{nuc}}(\Lambda_+ - \Lambda_-)$$

$$\Delta_{bottom} = -G_{bottom}AP + \frac{\langle E_e \rangle_{bottom}}{2M_{nuc}}(\Lambda_+ - \Lambda_-)$$

We have neglected the quadrupole term in the denominator $(N_+ + N_-)$, where it is smaller than the dominant term by four orders of magnitude. We have also generously assumed that the angular integration of $[(v/c)^2\cos^2\theta - (v/c)^2/3]$ is 1. The term $\langle E \rangle$ is the "average" positron energy, weighted by the Fermi integrand f(E). It differs between top and bottom to the extent that the energy cuts differ for the two detectors. The quantity Δ is:

$$\Delta = \Delta_{top} - \Delta_{bottom} = (G_{top} + G_{bottom})AP + (\Lambda_+ - \Lambda_-)\frac{\delta\langle E_e\rangle}{2M_{nuc}}$$

where $\delta\langle E\rangle = \langle E\rangle_{top} - \langle E\rangle_{bottom} \cong 0.5\text{MeV}$. This value is determined from the relative shift in the top and bottom energy spectra, which was about twenty channels. From the high energy calibrations, the energy change per channel is 0.018MeV, hence twenty channels represents an energy shift of about 0.4MeV. Thus we find, very conservatively assuming $(\Lambda_+ - \Lambda_-) = 100\%\langle\Lambda\rangle = 1$,

$$(\Lambda_+ - \Lambda_-)\delta\langle E_e\rangle/2M_{nuc} \cong (1/2\text{MeV})/(70\text{GeV}) \cong 7\times10^{-6}$$

which is completely negligible compared to GAP≥0.047.

H. Conclusion

Combining these corrections we obtain the final result for A_0. Because the uncertainties associated with the corrections are small compared to the statistical uncertainty in β_1 they are negligible when combined in quadrature. The final result is,

$$A_0 = 0.49 \pm 0.10$$

The final result agrees with the value $A_0 = 0.43 \pm 0.01$ calculated from the accepted value for G_v. This result is in marked disagreement with the old value,

measured on three previous occasions, $A_0 = 0.22 \pm 0.03$ (Ref.8). The derived value for the Cabibbo angle from this experiment is,

$$\theta_1 = 0.28 \pm 0.08 \text{ rad}$$

in agreement with all other beta decay measurements; equivalently, the derived value for the vector coupling constant G_v is

$$(1+\Delta_R)^{1/2} G_v = (1.397^{+0.026}_{-0.035}) \times 10^{-49} \text{ erg cm}^3$$

compared with the value

$$(1+\Delta_R)^{1/2} G_v = (1.4129 \pm 0.0004) \times 10^{-49} \text{ erg cm}^3$$

derived from the $0^+ \Rightarrow 0^+$ pure Fermi transitions.

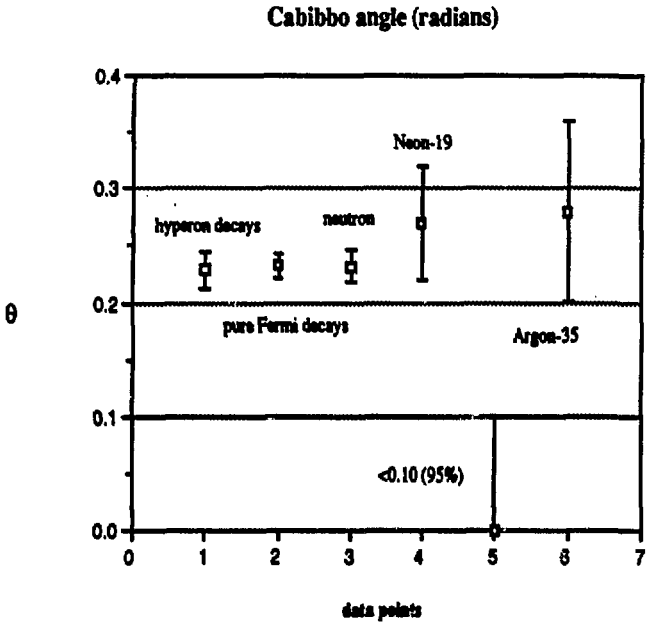

Figure 3: Graph of the Cabibbo angle determined from hyperon decays, pure $0^+ \Rightarrow 0^+$ Fermi decays, neutron decay, ^{19}Ne, and ^{35}Ar (including the previous weighted average and our new measurement).

references: (also see General references at the end of chapter two)

[1]Private communication, C. R. Hurlbut, Bicron Corporation

[2]T. Tabata, R. Ito, and S. Okabe, Nucl. Inst. and Meth., 94 (1971) 509

[3]National Academy of Sciences-National Research Council, "Studies in Penetration of Charged Particles in Matter", report #39, Nuclear Science Series (1964)

[4]P. J. Ebert, A. F. Lauzon, and E. M. Lent, Phys. Rev., 183 (1969) 422

[5]Kenneth A. Wright and John G. Trump, J. Appl. Phys., 33 (1962) 687

[6]V. A. Kuzminikh and S. A. Vorobiev, Nucl. Inst. and Meth., 129 (1975) 561

[7]Private communication, Eric B. Norman, Staff Scientist, Lawrence Berkeley Laboratory, Nuclear Science Division, Berkeley, CA

[8]F. P. Calaprice, E. D. Commins, and D. A. Dobson, Phys. Rev., 137B (1965) 1453 also:

F. P. Calaprice, University of California thesis, UCRL-17551 (1967) and W. C. Mead, Princeton University thesis (1974). The quoted result represents a weighted average. See reference 14, chapter one.

[9]B. Holstein and S. Treiman, Phys. Rev. C, C (1971)1921

Acknowledgements

Eugene Commins is not only a fantastic experimentalist but also a good human being. His patience, thoughtfulness, and humanity made graduate school a meaningful experience.

Thanks to Gene's other students: Persis Drell, Carol Tanner, Ivan Otero, and especially Kamal Abdullah for useful discussions and necessary excursions for coffee.

Thanks to Andy Brocatta and Tom Peterson for excellent machining; Laverne, Mason, and Ken for electronics help.

Thanks to Kevin Lesko and Rick Norman for helping to make our experiment a pleasant and successful finish. Thanks also to Sebastian Kuhn and Ruth Mary Larimer for unending help at the 88-Inch Cyclotron facility.

Many thanks to Deborah Towle-Shekter for encouragement and being my very good friend.

Special thanks to Jane Anne Phillips whose love and support helped me through the rough times.

Finally to my friends Peter Dingus, Arman Raphaelian, and Glenn Stark: the journey is almost finished, time to buy the wine and rendevous at that outdoor cafe in Europe!

This thesis is dedicated to my mother, Nina H. Garnett, who has worked so hard all of her life so that her children could succeed. Her love and happiness, even through the hard and painful times, has always been an inspiration to me.